Thesis for the degree of Licentiate of Engineering

High Spectral Efficiency Fiber-Optic Transmission Systems Using Pilot Tones

Mikael Mazur

Photonics Laboratory
Department of Microtechnology and Nanoscience – MC2
Chalmers University of Technology
Göteborg, Sweden 2018

High Spectral Efficiency Fiber-Optic Transmission Systems Using Pilot Tones

Mikael Mazur

Göteborg, May 2018

Technical report MC2 - 394
ISSN 1652-0769

Photonics Laboratory
Department of Microtechnology and Nanoscience – MC2
Chalmers University of Technology
SE-412 96 Göteborg
Sweden
Telephone: +46 (0)31-772 1000

Printed by Chalmers Reproservice, Chalmers University of Technology
Göteborg, Sweden, May 2018

High Spectral Efficiency Fiber-Optic Transmission Systems Using Pilot Tones

Mikael Mazur
Photonics Laboratory
Department of Microtechnology and Nanoscience – MC2
Chalmers University of Technology, SE-412 96 Göteborg, Sweden

Abstract

Modern fiber-optic communication systems combine state-of-the-art components with powerful digital signal processing (DSP) to maximize the system spectral efficiency (SE). Systems rely on wavelength-division multiplexing, including superchannel transmission, to enable transmission over the available bandwidth which reaches about 10 THz when accounting for the so-called C and L bands. A superchannel is a set of densely packed wavelength channels viewed as a single unit. By treating the channels together, they can be packed more closely than what is normally feasible and sharing of resources among the channels within the superchannel can be considered.

In this thesis we focus on the special case of superchannels formed using coherent optical frequency combs. A frequency comb is a multi-wavelength light source and comb-based superchannels consists of channels which are modulated on lines originating from a common comb. Frequency combs have phase-locked carriers, meaning that in contrast to the standard case of independent lasers, the channels within a comb-based superchannel are locked on a frequency grid. Moreover, it implies that the carrier offsets originating from a non-ideal laser source are shared among all comb lines.

Shared carrier offsets can be exploited to reduce the complexity of the DSP used to effectively recover the data. A frequency comb is fully characterized by knowing the state of two of its lines, meaning that if this information is transferred to the receiver, one could compensate carrier offsets for all wavelength channels within the superchannel. By transmission of optical pilot tones, self-homodyne detection of a 50×20 Gbaud PM-64QAM superchannel is demonstrated with 4% spectral overhead.

While two tones are required to fully phase-lock two combs, a single tone is enough to enable significant relaxation of the DSP-requirements while at the same time requiring minimal additional complexity compared to standard intradyne systems. Superchannel transmission using a single shared pilot tone is demonstrated by transmission of a 51×24 Gbaud PM-128QAM superchannel

with a resulting SE of 10.3 bits/s/Hz. The single pilot scheme is also evaluated for distances up to 1000 km showing high robustness to both noise and fiber nonlinearities. Finally, the high gain low overhead combination of the single pilot-tone scheme was used in a record demonstration reaching a SE of 11.5 bits/s/Hz for fully loaded C-band transmission.

Keywords: Fiber-Optic communication, Analog signal processing, Coherent communication, Coherent optical frequency combs

List of Papers

This thesis is based on the following appended papers:

[A] **M. Mazur**, A. Lorences-Riesgo, J. Schröder, P. A. Andrekson and M. Karlsson, "10 Tb/s self-homodyne PM-64QAM superchannel transmission with 4% spectral overhead", *Journal of Lightwave Technology* , DOI: 10.1109/JLT.2018.2820166, 2018.

[B] **M. Mazur**, A. Lorences-Riesgo, J. Schröder, P. A. Andrekson and M. Karlsson, "High Spectral Efficiency PM-128QAM Comb-Based Superchannel Transmission Enabled by a Single Shared Optical Pilot Tone", *Journal of Lightwave Technology* , Vol. 36, no. 6, pp. 1318 - 1325, 2018.

[C] **M. Mazur**, A. Lorences-Riesgo, J. Schröder, M. Karlsson and P. A. Andrekson, "Comb-Based Superchannel Transmission with Single Shared Optical Pilot", *Submitted to Optics Express*, 2018.

[D] **M. Mazur**, J. Schröder, A. Lorences-Riesgo, M. Karlsson and P. Andrekson, "11.5 bits/s/Hz PM-256QAM Comb-Based Superchannel Transmission by Combining Optical and Digital Pilots", *Proceedings of the Optical Fiber Conference (OFC)*, Paper. M1G.2, 2018.

Related publications and conference contributions by the author not included in the thesis:

Journal papers

[E] A. Fülöp, **M. Mazur**, A. Lorences-Riesgo, P-H. Wang, Xi Xuan, D. E. Leaird, M. Qi, P. A. Andrekson, A. M. Weiner and V. Torres-Company, "High-order coherent communications using mode-locked dark-pulse Kerr combs from microresonators",*Nature Communications* , Vol. 9, Paper. 1598, 2018.

[F] A. Fülöp, **M. Mazur**, A. Lorences-Riesgo, T. A. Eriksson, P-H. Wang, Xi Xuan, D. E. Leaird, M. Qi, P. A. Andrekson, A. M. Weiner and V. Torres-Company, "Long-haul coherent communiations using microresonator-based frequency combs",*Optics Express* , Vol. 25, no. 22, pp. 26678-26688, 2017.

[G] A. Lorences-Riesgo, **M. Mazur**, T. A. Eriksson, P. A. Andrekson and M. Karlsson "Self-homodyne 24×32-QAM superchannel receiver enabled by all-optical comb regeneration using Brillouin amplification",*Optics Express* , Vol. 24, no. 26, pp. 29714-29723, 2016.

[H] L. Lundberg, M. Karlsson, A. Lorences-Riesgo, **M. Mazur**, V. Torres-Company, J. Schröder and P. A. Andrekson Frequency Comb-Based Transmission Systems Enabling Joint Signal Processing",*Applied Sciences*, Special Issue: DSP for Next Generation Fibre Communication Systems, 2018.

Invited and upgraded conference papers and presentations

[I] A. Fülöp, **M. Mazur**, A. Lorences-Riesgo, P-H. Wang, Yi Xuan, D. E. Leaird, M. Qi, P. A. Andrekson, A. M. Weiner and V. Torres-Company"PM-64QAM Coherent Optical Communications Using a Dark-Pulse Microresonator Frequency Comb",*Proceedings of Conference on Lasers and Electro-Optics (CLEO)*, Paper. SW3C.1, 2018.

[J] A. Fülöp, **M. Mazur**, A. Lorences-Riesgo, T. A. Eriksson, P-H. Wang, Yi Xuan, D. E. Leaird, M. Qi, P. A. Andrekson, A. M. Weiner and V. Torres-Company, "Microresonator frequency combs for long-haul coherent communications",*International conference on Laser Optics (ICLO)*, 2018.

[K] **M. Mazur**, A. Lorences-Riesgo, Jochen Schröder, P. Andrekson and M. Karlsson, "10.3 bits/s/Hz spectral efficiency 54×24 Gbaud PM-128QAM superchannel transmission using single pilot",*Proceedings of European on Optical Communication (ECOC)*, Paper. M.1.F.5, 2017.

Regular conference presentations and papers

[L] L. Lundberg, **M. Mazur**, A. Fülöp, V. Torres-Company, M. Karlsson and P. Andrekson, "Phase Correlation Between Lines of Electro-Optical Frequency Combs",*Proceedings of Conference on Lasers and Electro-Optics (CLEO)*, Paper. JW2A.149, 2018.

[M] C. Fougstedt, L. Svensson, **M. Mazur**, M. Karlsson and P. Larsson-Edefors, "Finite-Precision Optimization of Time-Domain Digital Back Propagation by Inter-Symbol Interference Minimization,*Proceedings of European on Optical Communication (ECOC)*, Paper. W.1.D.2, 2017.

[N] L. Lundberg, **M. Mazur**, A. Lorences-Riesgo, M. Karlsson and P. Andrekson, "Joint carrier recovery for DSP complexity reduction in frequency comb-based superchannel transceivers",*Proceedings of European on Optical Communication (ECOC)*, Paper. Th.1.D.3, 2017.

[O] A. Fülöp, **M. Mazur**, A. Lorences-Riesgo, P-H. Wang, Xi Xuan, D. E. Leaird, M. Qi, P. A. Andrekson, A. M. Weiner and V. Torres-Company, "Frequency noise of a normal dispersion microresonator-based frequency comb",*Proceedings of the Optical Fiber Conference (OFC)*, Paper. W.2.A.6, 2017.

[P] **M. Mazur**, A. Lorences-Riesgo, M. Karlsson and P. Andrekson, "10 Tb/s self-homodyne PM-64QAM superchannel transmission with 4% spectral overhead",*Proceedings of the Optical Fiber Conference (OFC)*, Paper. Th.3.F.4, 2017.

[Q] C. Fougstedt, **M. Mazur**,L. Svensson, H. Eliasson, M. Karlsson and P. Larsson-Edefors, "Time-domain digital back propagation: Algorithm and finite-precision implementation aspects,*Proceedings of the Optical Fiber Conference (OFC)*, Paper. W.1.G.4, 2017.

[R] A. Fülöp, **M. Mazur**, T. A. Eriksson, P. A. Andrekson, P-H. Wang, Xi Xuan, D. E. Leaird, M. Qi, A. M. Weiner and V. Torres-Company, "Long-haul coherent transmission using a silicon nitride microresonator-based frequency comb as WDM source",*Proceedings of Conference on Lasers and Electro-Optics (CLEO)*, Paper. SMF.2, 2016.

[S] A. Lorences-Riesgo, T. A. Eriksson, **M. Mazur**, P. A. Andrekson and M. Karlsson, "Quadrature decompossion of a 20 Gbaud 16-QAM signal into 2×4-PAM signals",*Proceedings of European on Optical Communication (ECOC)*, Paper. Tu.1.E.3, 2016.

[T] T. Fehenberger, **M. Mazur**, T. A. Eriksson, M. Karlsson and N. Hanik, "Experimental analysis of correlations in the nonlinear phase noise in optical fiber systems",*Proceedings of European on Optical Communication (ECOC)*, Paper. W.1.D.4, 2016.

[U] **M. Mazur**, T. Taunay, T. Geisler, L. Gruener-Nielsen, M. Karlsson and P. A. Andrekson, "Measurements of temperature-induced polarization drift and correlation in a 7-core fiber",*Proceedings of European on Optical Communication (ECOC)*, Paper. W.1.B.2, 2016.

Other published work

[V] J. Schröder and M. Mazur," *QAMPy a DSP chain for optical communications*, DOI: 10.5281/zenodo.1195720, 2018.

Contents

Dedicated to my grandparents, Barbara and Georg B. Mazur

Acknowledgements

First, I would like to thank my examiner Prof. Peter A. Andrekson for accepting me as a PhD student and for your continuous support. My main supervisor, Prof. Magnus Karlsson, deserves endless thanks for always being open to discuss ideas, for your support and for giving me the opportunity to try out my own ideas. Many thanks to Dr. Jochen Schröder for accepting the role as supervisor and for convincing me to use Python. You have always taken your time to discuss my somewhat crazy ideas and encouraged me to push the boundaries and try out new things. Finally, my last supervisor, Dr. Abel Lorences-Riesgo deserve a special thank you for all your support. You taught me endless things about how it is to work in the lab and what it is like to do and present research. Working together with you is a true joy and and I will forever smile when thinking of Brillouin amplification.

Thank you Dr. Attila Fülöp for our interesting collaborations and for teaching me about micro-ring resonators. Many thanks to Christoffer Fougstedt for teaching me about hardware, to Lars Lundberg for fruitful discussions on joint DSP and to Dr. Elham Nazemosadat for always being open to share your deep knowledge on SDM. Special thanks to Emanuel Haglund and Ewa Simpanen for funny times together. Thank you all other colleges for contributing to an interesting working environment. Extra thank you to Jeanette Träff for your superb way of administrating the lab and for rescuing me when being lost in the jungle of administrative duties.

I would like to thank my friends outside the world of fiber-optic research for your support. Thank you all diving friends for our underwater experiences. Lena and Madeleine for our long-term friendship and your acceptance of my somewhat strange way of being. I would like to thank my family for your endless support and for your understanding of the many hours spent in the lab. Your never ending support means the most. Finally, my deepest thank you to Zoe for your love, acceptance and all the happiness you bring to me.

Chapter 1

Introduction

Technically, any form of communication using light falls under the optical communication umbrella, including the ancient use of smoke signals and Morse-signaling using light. Fiber-optic communication is a field within optical communication defined by the use of an optical fiber, typically together with a laser. The extraordinary achievements behind these technologies have been recognized on broad scale and in 1964, Charles H. Townes, Nicolay G. Basov and Aleksandr M. Prokhorov were awarded the Nobel price in physics for the innovation of the maser and the laser. More recently, in 2009, Charles K. Kao was awarded the price for the pioneering work on realizing the potential of optical fibers as a transmission medium.

Charles K. Kao's discoveries were published in 1966 [1] (reprinted 20 years later available in [2]) in which he realized that optical fibers at that time were loss-limited by impurities in the glass, not by intrinsic losses. Following this pioneering work, from around 1960 to around 1990, systems were mainly improved through improving the optical fiber, including going from multi-mode (MMF) to single-mode fibers (SMF). While it was clear that the lowest loss point for SMF was around 1550 nm, initial systems operated around 1310 nm to avoid penalties from dispersion which causes a walk-off between different spectral components of the transmitted signal.

Another major game-changer in the field of fiber-optic communication was the introduction of optical amplifiers in the telecommunication band (C-band) around 1550 nm [3]. Previously, system were limited to single-span and electrical regeneration. The invention of the Erbium-doped fiber amplifier (EDFA) changed this by allowing direct amplification in the optical domain [3]. To improve noise characteristics of EDFAs, much efforts were devoted to

developing pumping lasers around 980 nm [4, 5]. Major breakthroughs were achieved using high efficiency quantum well-based lasers [6] and application to EDFA pumping was investigated in [7]. The use of EDFAs boosted system experiments using solitons with propagation distances reaching 10000 km [8, 9].

While early systems transmitted around 1310 nm or relied on solition waveforms to avoid penalties from dispersion, a shift to 1550 nm was needed to exploit the potential for the combination of SMF and EDFAs. One solution was the dispersion-shifted fiber (DSF) with zero-dispersion around 1550 nm [10–12]. However, already at this time, most fiber deployed was SMF and upgrade-paths were sought to allow the use of already existing infrastructure. Optical dispersion compensation was therefore heavily investigated and a dispersion compensating fiber using a higher-order mode was proposed in [13]. Still, mode-shifting required additional components and was not fully compatible with the installed single-mode technology. The issue was solved in [14], with the introduction of the dispersion-compensating fiber (DCF). Following this, the potential for combining SMF, DCF and EDFAs for improving both system throughput and reach was quickly realized.

In addition to the low noise figure provided by EDFAs pumped around 980 nm, the EDFAs provided broad-band gain spanning the around 30 nm within the C-band. While wavelength-division multiplexing (WDM) previously had been demonstrated, the birth of the EDFAs and the development of DCF draw increased attention to research on WDM. Record experiments now targeted multi-span WDM transmission [15, 16]. With this new shift in system design, nonlinear effects started to be an increasingly limiting factor for systems and it was realized that the use of DSF represented a worst-case scenario by maintaining phase-coherence among channels over long distances, causing severe non-linear distortions [17, 18].

With the bandwidth of the C-band occupied using WDM, system design around late 1990 focused on the idea of coherent transmission using both the amplitude and the phase, together with advanced modulation formats to improve the spectral-efficiency (SE) beyond what was possible using previously techniques based on direct-detection (DD) [19]. Digital-to-analog converters (DACs) were first introduced in optical communication in 2005 when commercial transceivers capable of electronic pre-compensation of dispersion were introduced [20]. Three years later, analog-to-digital converters (ADCs) were added to the receiver [21]. The combination of transmitters with DACs and receivers with ADCs marks the starting point of coherent optical communication systems using digital signal processing (DSP) implemented in high-speed

application-specific integrated circuits (ASICs) [22, 23].

Early experiments using differential quadrature phase shift keying (D-QPSK) using optical delay-based receivers marks an early start of experiments using coherent formats [24]. As both laser quality and DSP performance improved, differential formats were replaced with coherent detection using a free-running local-oscillator (LO) and modulation order grew quickly [19]. With the introduction of coherent technologies, the optical communication community also started to increasingly connect with the fields of communication and information theory [25], applying advanced modulation and forward error correction (FEC) coding schemes to improve transmission performance. While the required bit to error ratio (BER) target of around 10^{-15} have been remained untouched throughout the years of development, these schemes have enabled new ways of ensuring the performance [26]. Simply replacing the use of on-off keying (OOK) with binary phase shift keying (BPSK) results in a 3 dB sensitivity gain [27].

Today, SMF with 0.14dB/km loss have been demonstrated [28] and formats reaching 4096-QAM are being evaluated in optical communication systems [29, 30]. In single-span Raman-amplified experiments, SE exceeding 17 bits/s/Hz have been demonstrated using low baud-rate carriers [31]. A SE of 14.1 bits/s/Hz over 500 km of Raman-amplified link was demonstrated in [32]. Combining state-of-the-art communication techniques using rate-adaptive FEC [33, 34], constellation shaping [35] and powerful DSP to combat both linear and non-linear impairments [36], system throughput have reached 25.4 Tb/s after 10284 km [37]. Adding EDFAs with capabilities of L-band amplification, state-of-the-art results exceed 70 Tb/s system throughput over 7600 km [38] and 51 Tb/s over 17000 km [39]. DAC and ADC bandwidth (BW) have improved tremendously over the years and record demonstrations include a 100 GHz BW DAC [40] and a >110 GHz BW ADC [41]. As a result of this, record symbol-rate is now reaching 180 Gbaud [41] and PM-1024QAM at 66 Gbaud have been demonstrated using powerful FEC [42]. Component performance are also increasing fast and the benefit of integration is clearly entering the domain of optical communication with fully integrated multi-channel transmitters reaching 100 Gbaud [43].

With all these improvements, concerns are raising that we are running out of capacity in SMF [44]. The actual capacity of the fiber channel (capacity is strictly defined in information theory [25]) is still unknown and research efforts are ongoing to produce better bounds [45–47]. Such lower bounds have shown that the capacity do not decay at high launch power but instead flattens out [46]. However, even if there are plenty of capacity left, it is becoming

increasingly challenging to exploit the full capacity of SMF transmission technologies beyond what is reachable in the linear or quasi-linear regime. As a matter of fact, optical transmission system relies more or less fully on linear communication theory developed for completely different channels to the optical one, although similarities in the behavior of the distortions makes it possible.

As a concluding remark on the development, one have to mention the introduction of space-division multiplexing (SDM) [48, 49]. These system relies on increasing the number of parallel paths used for multiplexing of data by considering the use of orthogonal sets of modes, the use of fibers with several cores, or several independent transmission fibers. SDM technologies has enabled current record throughput exceeding 10 Pb/s [50] over a 10 km fiber containing 19 cores, each supporting 6 modes. System throughput of 159 Tb/s over 1045 km using 3-mode transmission was demonstrated in [51] and simultaneous transmission over 15 spatial modes was demonstrated in [52]. Moreover, recent results using few-mode fiber (FMF) [53] and coupled-core multi-core fiber (CC-MCF) [54] have shown that the use of SDM-fibers can outperform classical SMFs by providing additional gain due to improved tolerance to fiber nonlinearities. However, while SDM have been successful in enabling record-breaking transmission results, lots of work remains before its fully understood how to use SDM technology. Similar to the criticism against the first DCFs based on FMF, SDM requires deploying completely new networks with potential unknown risks.

1.1 This Thesis

This thesis is focused around superchannels with high SE enabled by combining frequency combs with optical pilot tones. A superchannel is a set of densely packed channels which are treated as a unit, removing the need to dedicate guard-bands required to be able to optically separate the channels from each other. Here, we focus on the special case of superchannels in which all channels are modulated on lines originating from an frequency comb. One key implication of this assumption is that carrier offsets are shared among all channels within the superchannel. In addition, full knowledge of these carrier offsets can be gained by using information from only two comb lines.

We propose to transmit unmodulated pilot tones within the comb-based superchannels which are recovered at the receiver. The receiver is also based on a frequency comb and by locking the receiver comb to the incoming pilot(s) carrier offsets can be compensated. If two pilot tones are transmitted, the

receiver comb can be phase-locked to the incoming pilot tones, enabling self-homodyne detection with low spectral overhead. This was experimentally demonstrated in Paper A, resulting in a spectral overhead of 4% for self-homodyne detection. While two pilot tones allows for full characterization, a single pilot tone can lead to significant offset reduction. This was demonstrated in Paper B, demonstrating state-of-the-art SE by using a single shared optical pilot tone to facilitate blind DSP in superchannels with high-order modulation formats. Paper C investigates the sensitivity to the proposed scheme using pilot tones for transmission distances up to 1000 km. Finally, in Paper D, the single pilot tone scheme is used in a high SE experiment, establishing a new record SE of 11.5 bits/s/Hz for full C-band transmission.

Chapter 2

Optical Communication Systems

An overview over a single channel optical communication system can be seen in Fig. 2.1. From a systems perspective, an optical communication system can be divided into three key parts; transmitter, optical channel and the receiver. While highly linked together, key distinctions still separate them and important details are outlined in the following sections.

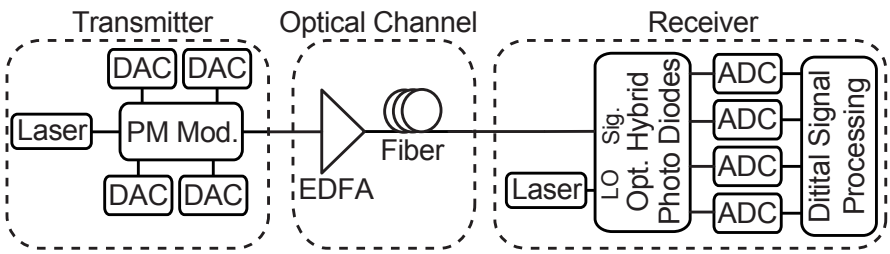

Fig. 2.1. Overview of a optical communication system. DACs are used to convert information symbols from the digital to main to electrical signals which are modulated onto the lightwave carrier using an optical modulator. After propagation through the link consising of spans with optical fiber and optical amplifiers, the signal is detected using a optical receiver. The receiver consist of an optical hybrid and balanced detectors, enabling detection of both the amplitude and the phase of the incoming lightwave. After sampling using the receiver ADCs, advanced DSP is used to recover the data.

2.1 Transmitter

The role of the transmitter is to encode the information onto the optical carrier wave. Its operation can roughly be divided into functions implemented in the digital, electrical and optical domain. Operations in the digital domain are characterized by discrete-time representations of bits or complex symbols with a fixed oversampling value. This discrete digital signal is then converted to continuous analog electrical signals through the use of DACs. The resulting signal spectrum is then DC-centered. Finally, an optical modulator is used to attach the electrical signal to its optical carrier wave, resulting in an effective up-conversion of the signal spectrum from being DC-centered to being centered around the optical carrier wave frequency.

2.1.1 Digital Bit-Symbol Mapping

To transmit a sequence of bits, the first step is to add redundant bits using the FEC encoder. However, here we only focus on sending bits and therefore only consider the case of a bit sequence which shall be transmitted over the system, neglecting any detailed discussions on FEC encoders. Bits are then mapped to symbols, which can carry one or more bits, a processed referred to as mapping. Each symbol $a[n]$ (n denoting the time index) is a 2D symbol and can have bits mapped onto two quadratures. The interpretation of these two quadrature can be seen as mapping the bits to symbols belonging to a (sub)-space spanned by both the amplitude and phase of the optical lightwave, resulting in a 2D signal space. The selected constellation point in this signal space is then represented by the complex value $a[n]$. Similarly, considering polarization multiplexing (PM) using two quadratures on two polarization, the signal space is 4D which can be understood by combining two complex symbols $a[n]$ according to

$$\vec{a}_{\mathrm{PM}} = \begin{pmatrix} a_X[n] \\ a_Y[n] \end{pmatrix}. \tag{2.1}$$

While one in practice can use a continuous modulation alphabet (and this is shown to be capacity achieving for certain distributions), we often want to use a finite set of "symbols" to represent the bit stream. Considering a 4D signal spaces spanned by using the two quadratures on two orthogonal polarizations, optimized modulation can be used to maximize performance [55–57]. However, in practise formats such as PM M-ary quadrature amplitude modulation (PM-M-QAM) are mostly used. These formats map independent QAM symbols on

each polarization. The two quadratures of each QAM symbol is furthermore separated into two 1D pulse amplitude modulation (PAM) signals. So to map a bit stream onto PM-M-QAM symbols, the bits are divided into 4 sub-streams, each mapping the bits to a 1D PAM constellation. The number of bits N_b encoded in each symbol is directly given by $N_b = \log_2(M)$ with M being the format order. As an example, a PM-64QAM symbol carriers a total of 12 bits, 6 bits on each polarization, corresponding to symbol alphabet of size $2^6 = 64$. Each 64QAM symbol consists furthermore of two independent PAM signals, modulating 3 bits each, corresponding to $2^3 = 8$ levels or equivalent a 8-PAM signal. A PM-64QAM symbol can therefore be decomposed into four individual real-valued 8-PAM signals.

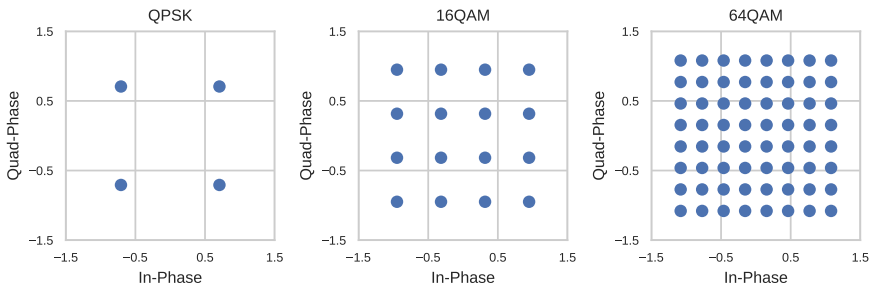

Fig. 2.2. Example of coherent modulation formats used in optical communication. The number of bits encoded in each M-QAM symbol is given by $N_b = \log_2(M)$, corresponding to $N_b = 2{,}4$ and 6 for the case of QPSK, 16QAM and 64QAM, respectively.

Focusing on the complex representation of the 2D symbols $a[n]$, Fig. 2.2 shows the resulting constellation diagrams for $M = 4{,}16$ and 64, corresponding to QPSK, 64QAM and 64QAM, respectively. To decide on which complex constellation symbol to send, the bit stream is divided into blocks of N_b bits and a look-up-table with a the mapping. An example of such a mapping for 16QAM can be found in Table 2.1.

As a final remark to modulation it is important to point out that when considering an AWGN channel (see Section 2.2.1), the optimal modulation

Bit Sequence	Output Symbol
{0,0,1,0}	$(-3+3j)$
{0,0,1,1}	$(-3+1j)$
{0,0,0,1}	$(-3-1j)$
{0,0,0,0}	$(-1+3j)$
{0,1,1,0}	$(-1+1j)$
{0,1,1,1}	$(-1-1j)$
{0,1,0,1}	$(-1-3j)$
{1,1,1,0}	$(1+3j)$
{1,1,1,1}	$(1+1j)$
{1,1,0,1}	$(1-1j)$
{1,1,0,0}	$(1-3j)$
{1,0,1,0}	$(3+3j)$
{1,0,1,1}	$(3+1j)$
{1,0,0,1}	$(3-1j)$
{1,0,0,0}	$(3-3j)$

Table 2.1. Bit sequence to complex symbol mapping for 16QAM, $N_b = 4$. The selected mapping is of Gray-type (not unique).

format is a continuous Gaussian distribution. Recently, large research efforts have been focusing on constellation shaping to improve performance. This aims at exploiting the 1.53 dB asymptotic difference between the AWGN capacity (Eq. 2.8) and the use of QAM formats [58]. Shaping can be implemented either by symbols with a non-uniform probability, refereed to as probabilistic amplitude shaping (PAS) [35] or by redistributing the constellation symbols spherically in constellation space [38] which is known as geometric shaping. While constellation shaping has been used in several recent record experiments [29, 31, 37, 38], the work in this thesis is focused around standard QAM formats and we therefore do not consider shaping further throughout this thesis. However, all presented techniques are fully compatible with shaping and such techniques can hence be used to improve flexibility of the proposed systems.

2.1.2 Pulse Shaping

After mapping the bit sequence to complex symbols (1 per polarization mode), a pulse shaping filter is often used shape the signal to the modulator [59, 60].

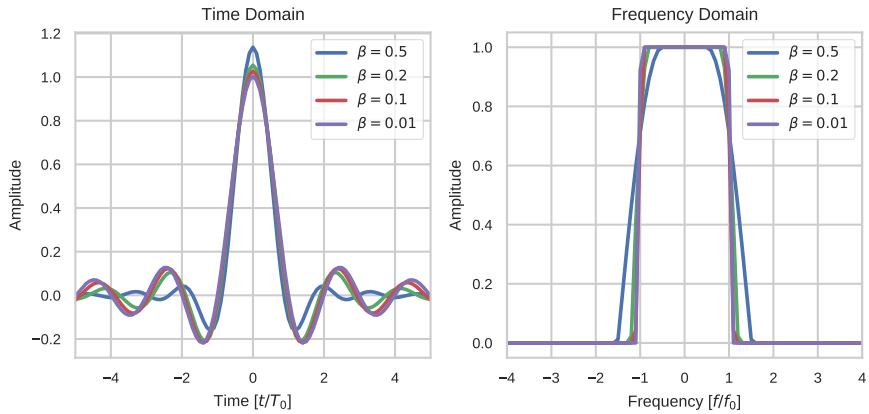

Fig. 2.3. Raised Cosine filtering with varying roll-off factor β. (a) shows the time-domain impulse response and (b) the equivalent representation in frequency domain.

This process can be expressed as [61]

$$x[n] = \sum_{k=-\infty}^{\infty} a[n-k]h[k], \tag{2.2}$$

where $x[n]$ is the output discrete waveform a time instance n, $a[n]$ is the selected complex symbol and h denotes the filter. Equation 2.2 represents a discrete convolution between the symbols $a[n]$ and the filter $h[n]$. Several different filters can be used but raised-cosine filters (RC) are among the most common. The RC filter can be seen as an approximation to the sinc-filter, providing a brick-wall filter response in frequency domain. The impulse response of the RC filter can be expressed according to [61]

$$h(t) = \begin{cases} \dfrac{\pi}{4T_0}\mathrm{sinc}\left(\dfrac{1}{2\beta}\right), & t = \pm\dfrac{T_0}{2\beta} \\ \mathrm{sinc}\left(\dfrac{t}{T_s}\right)\dfrac{\cos\left(\frac{\pi\beta t}{T_s}\right)}{1-\frac{4\beta^2 t^2}{T_0^2}}, & \text{otherwise} \end{cases}, \tag{2.3}$$

with T_0 denoting the symbol period and β the roll-off factor. Note that Eq. 2.3 results in a sinc function for the special (but idealized) case of $\beta = 0$.

The time and frequency response of the RC filter for $\beta \in 0.01,0.1,0.2,0.5$ can be seen in Fig. 2.3. Worth noticing here is that in order to apply a pulse shaping filter, oversampling is needed and the vector with complex symbols is therefore typically up-sampled at this point. While Fig. 2.3 shows the filter shape, the direct implication for signaling can be seen in Fig. 2.4, showing the resulting spectrum of a 16QAM signal with and without the use of an RC filter. Considering systems transmitting data on several wavelengths using WDM (see Section 4.1), the use of RC filters can enable much more effective use of the available signal spectrum.

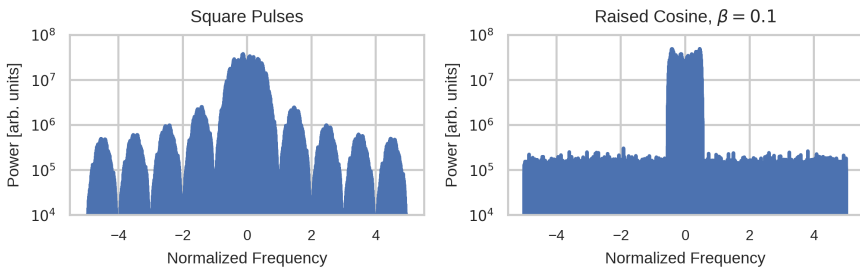

Fig. 2.4. Example of output signal spectrum for (a) an unshaped signal with square pulses in time domain and (b) a signal with a $\beta = 0.1$ RC filter.

2.1.3 Digital-to-Analog Conversion

After modulation and pulse-shaping, which both takes place in the digital domain, it is necessary to convert the digital signal representation into a continuous analog signal which can be modulated on the optical carrier. In the ideal case, the digital-to-analog conversion do not add any penalty but all real-life DACs have a limited resolution. For high-speed DACs used in optical communication, the limited resolution limits the performance for multi-level modulation formats [22].

The limited resolution can be understood by considering that a DAC has N different levels used to represent the digital signal which is expressed in bits (and hence also have a finite resolution). The DAC is controlled by a sampling clock and each discrete sample is held for a sampling period T_{Fs}. For each sample of the digital input signal, the DAC chooses the closest discrete representation and output the corresponding signal amplitude. Due to the quantization, penalties will arise as the output signal differs from the

original signal. This can be seen in Fig. 2.5(a), illustrating the implications of quantization for a sine-wave. How this quantization error is affecting a shaped data signal can be seen in Fig. 2.5(b), showing the frequency response of a RC-shaped signal. We observe that the noise-floor is about 1 order of magnitude higher for the quantized signal, compared to the floating-point representation.

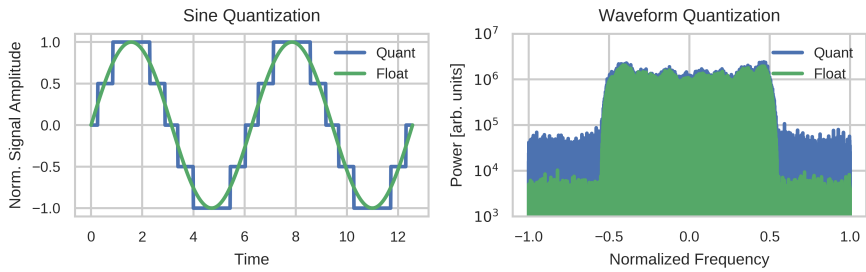

Fig. 2.5. (a) Quantization explained using a sine-wave as example. (b) shows additional noise added to a shaped waveform as a result of limited DAC resolution.

In practise DACs are not ideal and in addition to the limited resolution, presence of both noise and bandwidth limitations effectively reduce the number of equivalent bits. This is often characterized in terms of effective number of bits (ENOBs) which assumes a random approximation in the quantization error [62]. The combination of DAC resolution and ENOB can therefore be used to describe the quality of the output signal, including noise from the DAC itself.

2.1.4 Optical Modulation

Information can be modulated onto the light wave using either direct modulation of the laser (switching on-off) or via an external modulator applied after the laser [27]. Until the coherent era, data was modulated using on-off keying (OOK) [63]. Today, direct modulation of integrated lasers is still the base for short-reach optical interconnects [64].

To enable modulation beyond OOK, IQ-modulators are normally used. While requiring a more stringent optical alignment, IQ-modulators use interferometer structures to encode information. The most commonly used is the Mach-Zehnder modulator (MZM), typically based on $LiNbO_3$. Recent

work on integrated $LiNbO_3$ has showed bandwidth of 100 GHz [65]. While $LiNbO_3$ is the most commonly used platform for stand-alone modulators, other materials considered includes silicon [66], InP [67] and plasmonic modulators using gold substrates [68, 69]. Combining two MZMs and a $\pi/2$ optical phase shifter allows for independent modulation of the two quadratures of an optical lightwave [27]. Modulation can then be understood as up-conversion of shaped signal (Eq. 2.2) according to

$$A(t) = \sum_n a[n]h(t - nT_s)\exp(j\omega_0 t), \tag{2.4}$$

with ω_0 denoting the angular frequency of the optical carrier. In the case of modulating data onto both polarizations, the modulation process is done using a PM-modulator. The modulator is then built up of two separate IQ-modulator together with a polarization beam combiner to allow for simulations modulation onto all four degrees of freedom in a single-mode fiber at a single wavelength. The modulated output field is then controlled by changing the driving voltages to the four individual MZMs within the PM-modulator.

2.2 The Optical Fiber Channel

The optical fiber channel consists of the optical fiber medium and the amplifiers used to periodically amplify the signal in multi-span links. Several different kinds of fibers can be used for data transmission, depending on operating wavelength and practical demands. While short-reach optical interconnects typically use a graded-index MMF, high-throughput communication systems normally rely on the use of SMF and operation in the C-band (around 1550 nm).

Focusing on the fiber channel, signal distortions arise from propagation in the waveguide as well as from optical amplifiers along the link. Several amplification schemes exits such as EDFAs, distributed Raman amplification, parametric amplifiers [70] and semiconductor optical amplifiers [71]. Any detailed amplifier comparison is beyond the scope of this thesis and here we solely focus on the use of EDFAs. EDFAs relies on pumping a doped fiber segment at the Erbium transition wavelengths of around 980 nm and 1480 nm, based on the same principle as any laser.

The EDFA noise properties is often characterized by its noise figure (NF), F_n which is a measure of the signal quality degradation from amplification. It is defined as [72]

$$F_\mathrm{n} = 2n_\mathrm{sp}\frac{G-1}{G}, \tag{2.5}$$

where N_{sp} is the amplifier spontaneous emission factor which, for EDFAs, is $n_{\text{sp}} \geq 1$ and G denotes the amplifier gain. The implication of $n_{\text{sp}} \geq 1$ is that all EDFAs have a theoretical minimum NF of 3 dB, being limited by quantum mechanics [73]. Assuming a large gain which do not depend on frequency, the noise figure can be translated into an equivalent power spectral density (PSD) of

$$P_{\text{ASE}}(\omega) = \frac{F_{\text{n}}}{2} G\hbar\omega \qquad [\text{W/Hz}], \tag{2.6}$$

with $\hbar$ denoting Planck's constant and ω the angular frequency. Based on the key role of EDFAs together with understanding from Eq. 2.6 it is natural to understand the importance of models which considers additive white Gaussian noise (AWGN) contributions. Such models and their extensions to more complex fiber models are introduced in the upcoming sections.

2.2.1 The AWGN Fiber Channel Model

The simplest discrete model for fiber transmission can be stated as

$$y[n] = x[n] + N[n], \tag{2.7}$$

where $y[n]$ denotes the received symbol, $x[n]$ the transmitted one and $N[n]$ additive white Gaussian noise (AWGN). While not representing the full fiber channel, the AWGN fiber channel can still be used as a simple reference when designing DSP and performance is often referenced to the theoretical case of transmission over an AWGN channel. Worth pointing out here is also that the AWGN channel is one of few channels with a known channel capacity given by [25]

$$C = \log_2\left(1 + \frac{P_s}{N_0}\right) \qquad [\text{bits/s/Hz}], \tag{2.8}$$

with C denoting the channel capacity, P_s the signal power and N_0 the noise variance, defined according to

$$P_s = \mathbb{E}\left[|x[n]|^2\right], \tag{2.9}$$

$$N_0 = \mathbb{E}\left[|N[n]|^2\right], \tag{2.10}$$

with $\mathbb{E}$ denoting the expected value operator. The term $\frac{P_s}{N_0}$ is the signal to noise ratio (SNR) and Eq. 2.8 is therefore often expressed as $C = \log_2(1 + \text{SNR})$. The channel capacity, C, denotes the highest rate at which information can be communicated over the channel with arbitrary small error probability [25].

2.2.2 The Dispersive Fiber Channel

As discussed in Section 1, dispersion is a key aspect for the fiber channel. While being inherent in waveguide design, the dispersion causes different spectral components of the modulated channel to walk-off with respect to each other. The result is a bandwidth-distance-dependent fading which, if left without care, limits the system performance. To include dispersion, we move from looking at individual complex symbols $a[n]$ to looking at the electrical field envelope $A(z,t)$ defined by Eq. 2.4. The effect of dispersion can then be modelled as [72]

$$\frac{\partial A}{\partial z} + \beta_1 \frac{\partial A}{\partial t} + \frac{j\beta_2}{2}\frac{\partial^2 A}{\partial t^2} + \frac{\alpha}{2}A = 0, \tag{2.11}$$

with z denoting the propagation direction, β_1 denoting the group velocity inside the fiber, β_2 the second order dispersion and α the fiber loss. Since we are typically not interested in propagation with respect to a fixed point in space, we can reformulate Eq. 2.11 by considering a co-moving reference system (a reference system in which the observer is sitting centralized on the pulse A and follows it during propagating) according to

$$\frac{\partial A}{\partial z} + \frac{j\beta_2}{2}\frac{\partial^2 A}{\partial t^2} + \frac{\alpha}{2}A = 0. \tag{2.12}$$

Solving Eq. 2.12 is usually done in the frequency domain and since the loss term only reduces the amplitude of the pulse, we make a variable substitution according to $U(z,t) = \frac{A(z,t)}{\exp(-\alpha z/2)}$ and insert it into Eq. 2.12 which reduces to

$$\frac{\partial U}{\partial z} + \frac{j\beta_2}{2}\frac{\partial^2 U}{\partial t^2} = 0. \tag{2.13}$$

Taking the Fourier transform of Eq 2.13 then results in

$$\frac{\partial U(z,\omega)}{\partial z} = j\frac{\beta_2\omega^2}{2}U(z,\omega). \tag{2.14}$$

Equation 2.14 is a first order ordinary differential equation in z and can be solved according to

$$U(z,\omega) = \exp\left(j\frac{\beta_2\omega^2 z}{2}\right)U(0,\omega). \tag{2.15}$$

From Eq. 2.15, the effect of dispersion can be understood as a parabolic phase response in frequency domain. Given that the inverse Fourier transform of a phase shift is a time delay, dispersion simply broadens a pulse in time as it propagates along the fiber.

2.2.3 The Nonlinear Fiber Channel

In addition to the linear channel response described by Eq. 2.12, the optical fiber also has a nonlinear response from the silica glass. The implication of this is an intensity dependent refractive index which can be written as [72]

$$n_{\text{Eff}} = n_0 + n_2 I, \tag{2.16}$$

with n_{Eff} being the resulting, n_0 the linear, and n_2 the nonlinear refractive index coefficient, respectively. In Eq. 2.16, I denotes the intensity of the electric field which gives raise to the nonlinear interaction. The effect of a nonlinear refractive index can then be viewed as a power-dependent modulation of the refractive index in the fiber. Incorporating such effects in our channel model relies on considering the nonlinear polarization response of the electrical displacement field and solving Maxwell's equations for fiber propagation. A more detailed derivation is beyond the scope of this thesis, but can be found in [72].

Including the nonlinear effect, known as Kerr nonlinearity, into Eq. 2.13, results in the famous nonlinear Schrödinger equation for fiber optics, according to [72]

$$\frac{\partial A}{\partial z} + \frac{j\beta_2}{2}\frac{\partial^2 A}{\partial t^2} + \frac{\alpha}{2}A = j\gamma|A|^2 A, \tag{2.17}$$

with γ being the nonlinear coefficient of the optical fiber. Equation 2.17 has no analytical solution and numerical methods are required approximate the solution in the general case. However, important insights to the implications of fiber nonlinearities can be found by considering the case of a channel without dispersion, i.e. $\beta_2 = 0$. Substituting $U(z,t) = \frac{A(z,t)}{\sqrt{P_0}\exp(-\alpha z/2)}$, with P_0 denoting the pulse peak power, an analytical solution to Eq. 2.17 can be found according to

$$U(z,t) = U(0,t)\exp(j\phi_{\text{NL}}(z,t)). \tag{2.18}$$

The term ϕ_{NL} is often refereed to as the nonlinear phase shift given by

$$\phi_{\text{NL}} = |U(0,t)|^2 \gamma P_0 \int_0^z \exp(-\alpha z')dz'. \tag{2.19}$$

At first glimpse, Eq. 2.19 can look a bit confusing and to ease the understanding it is convenient to introduce two additional length scales known as the nonlinear

length L_{NL} and the effective length L_{Eff}, defined according to

$$L_{\mathrm{NL}} = \frac{1}{P_0 \gamma} \tag{2.20}$$

$$L_{\mathrm{Eff}} = \int_0^z \exp(-\alpha z')dz' = \frac{1-\exp(\alpha z)}{\alpha} \tag{2.21}$$

Introducing L_{NL},L_{Eff}, Eq. 2.19 changes to

$$\phi_{\mathrm{NL}}(z,t) = |U(0,t)|^2 \frac{L_{\mathrm{Eff}}}{L_{\mathrm{NL}}}, \tag{2.22}$$

and we can understand the Kerr nonlinearity as a phase-shift in time domain which depends on the pulse shape as well as the relation between the nonlinear and effective length. Note that $\phi_{\mathrm{NL}}(z,t)$ is directly proportional to the optical power and a way of increasing or decreasing the amount of nonlinearities is therefore simply to adjust the optical power. A final important remark on fiber nonlinearities is that while both nonlinear and dispersive effects give raise to a phase shift, the implications are very different. Dispersion is an inherently linear effect in which the phase shift is dependent on the frequency content. In contrast, nonlinearities depend on the profile in time and the phase shift there causes spectral broadening and transfer of energy among different spectral components within the pulse.

2.2.4 The Gaussian Noise Model

While numerical solution of the nonlinear Schrödinger equation provides a way of estimating system performance using simulations, brute force solutions is computationally heavy. As a result of this, large efforts have been devoted to developing simpler models with the most famous one being the Gaussian noise model (GN-model) [74–76].

The GN-model focus on uncompensated transmission systems in which the signal can be assumed to be highly dispersed. As given away by the name, the model therefore assumes that the signal can be approximated with a Gaussian distribution and that the nonlinear penalty can be approximated with an extra noise term so that the SNR is expanded according to [75]

$$\mathrm{SNR} = \frac{P_S}{\sigma^2_{\mathrm{ASE}} + \sigma^2_{\mathrm{NL}}}, \tag{2.23}$$

with $\sigma^2_{\mathrm{ASE}}, \sigma^2_{\mathrm{NL}}$ being the variance of the amplifier noise and the nonlinear noise-like distortions, respectively. For uncompensated transmission, the

model has proven accurate over a broad range of fiber types and transmission distances [77]. Worth emphasizing though is that the GN-model assumes that the signal is a Gaussian process and is hence modulation format independent. However, an extended version, the extended GN-model (EGN-model) accounts for this at the expense of a more complicated model [78].

2.2.5 Polarization-Dependent Channel Models

As discussed before, the fundamental mode in a SMF is polarization degenerate. However, the circular symmetry of a transmission fiber is non-ideal in practise and small fiber birefringence causes polarization rotations as well as give raise to effects such as polarization mode dispersion (PMD) and polarization dependent loss (PDL). Lots of work have been focusing on understanding the effect of mainly PMD which, before the introduction of coherent DSP limited system reach [79–81]. Without going into detail, we only focus on two separate models for dual-polarization transmission.

The first is an extension from the classical AWGN channel by including a polarization scattering matrix H. Equation 2.7 can then be expanded according to

$$y[n] = Ha[n] + N[n], \tag{2.24}$$

with H being a 2×2 complex value unitary matrix in the case of no PDL . If PMD is present H is frequency dependent and the matrix product in Eq. 2.24 will be a convolution with $a[n]$.

Several ways exists for including polarization dependence along the propagation, depending on how the polarization is treated. Focusing on communication over longer distances of fiber (spanning km), the Manakov model is commonly used [17]. In the Manakov model, the state-of-polarization is averaged over the Poincare sphere (Stokes representation [82]), leading to a famous extension of Eq. 2.17 according to [83]

$$\begin{aligned} \frac{\partial A_x}{\partial z} + \frac{j\beta_2}{2}\frac{\partial^2 A_x}{\partial t^2} + \frac{\alpha}{2}A_x &= j\gamma\frac{8}{9}\left(|A_x|^2 + |A_y|^2\right)A_x, \\ \frac{\partial A_y}{\partial z} + \frac{j\beta_2}{2}\frac{\partial^2 A_y}{\partial t^2} + \frac{\alpha}{2}A_y &= j\gamma\frac{8}{9}\left(|A_x|^2 + |A_y|^2\right)A_y. \end{aligned} \tag{2.25}$$

2.3 Optical Receiver

The role of the optical receiver is to extract the information carried by the optical carrier and to retrieve the encoded information. This process involves

several steps including down-conversion, detection, digitizing and DSP.

As outlined in Fig. 2.1, the incoming signal is mixed with a second laser, the LO, in a coherent optical receiver. Coherent detection is nothing new and has been used for decades within the wireless community. Within the field of optical communication, "lack of high speed ADCs and powerful DSP ASICs" meant that it took more than 20 years after the introduction of optical communication systems until the coherent era started.

2.3.1 Optical Receiver Front-End

Coherent detection refers to the process of detecting both the amplitude and phase of the light wave envelope. In this, the optical phase is extracted with the LO as reference by mixing it using an optical hybrid in which one arm is delayed $\pi/2$ with respect to the other one. The result is two output signal which can be combined two and two using balanced photo detectors to produce output photo-currents according to [84]

$$\begin{bmatrix} i_I(t) \\ i_Q(t) \end{bmatrix} \propto \begin{bmatrix} \mathrm{Re}\left(E_{\mathrm{Sig}}(t)E^*_{\mathrm{Lo}}(t)\right) \\ \mathrm{Im}\left(E_{\mathrm{Sig}}(t)E^*_{\mathrm{Lo}}(t)\right) \end{bmatrix}, \tag{2.26}$$

with $i_{I,Q}$ denoting the resulting electrical currents representing the in-phase and the quadrature-phase of the modulated envelope, $E_{\mathrm{Sig}}(t)$ denoting the input signal field and E_{Lo} denoting the LO field.

Similarly to how two separate IQ-modulators can be used to built up a PM modulator, two separate optical hybrids combined with a polarization beam splitter can be used to create a dual-polarization receiver. In such, Eq. 2.26, is expanded with indices to denote the X,Y polarization and the hybrid has four outputs.

2.3.2 Analog to Digital Conversion

After coherent detection using the optical hybrid, the resulting photo-currents needs to be sampled in order to produce a received signal in the digital domain. This is done by a set of high-speed ADCs, converting the photo-current into a sampled digital signal. As previously mentioned, optical systems are more to a large degree limited by the performance of the DACs and ADCs used in the transceivers [22].

Important aspects when characterizing an ADC is the number of bits, or equivalently, the resolution of the ADC, similarly to the DAC. While DAC and ADC design differ significantly, the metrics used to characterize them as

well as the implications of limited resolution on optical communication is very similar. The sample principles as outlined for the DACs in Section 2.1.3 can therefore be applied to the case of ADCs as well.

Chapter 3

Digital Signal Processing and Forward Error Correction

After transmission through the optical channel, the coherent optical receiver uses advanced DSP and powerful FEC to ensure reliable communication. The role of the DSP is to compensate for various signal impairments such as bandwidth limitations and polarization effects. In addition, the receiver implement a matched filter to maximize the probability of correct detection. Following this, FEC (or transmission of redundant data in clever ways) is used to ensure that the resulting error probability is below a selected threshold, often taken to be a BER of $< 10^{-15}$.

In the following descriptions of all algorithms we consider a received signal $r'(t) = I'(t) + jQ'(t)$, denoting the received signal with the impairment(s) under consideration. The corresponding output signal after processing is denoted $r(t) = I(t) + jQ(t)$. While there exists default schemes outlining the order in which the signal should be processed (see for example [60]), this is not necessarily fixed and some steps can be moved around to gain performance or ease the processing requirements. Example of this can be to group processes done in the frequency domain to minimize the number of consecutive Fourier transforms needed in a hardware implementation. Due to this, the following sections describes typical DSP algorithms used without strictly enforcing an order in which they shall be used.

3.1 Front-End In-Balance Compensation

Both the optical hybrid and the transmitter modulator can suffer from skew and in-balance between the I and Q component of the modulated and/or detected signal, causing distortions which leads to reduced performance [85, 86]. In-balance can be modeled according to [87],

$$\begin{aligned} r'(t) &= \left[g_I I\left(t-\frac{\tau_{IQ}}{2}\right)+o_i\right]+\left[g_Q Q\left(t+\frac{\tau_{IQ}}{2}\right)+o_Q\right]\exp\left(j\left(\frac{\pi}{2}+\phi_{IQ}\right)\right) \\ &= I'(t)+jQ'(t), \end{aligned} \tag{3.1}$$

with $r(t)$ denoting the received complex signal with $I'(t) = \mathrm{Re}\left(r'(t)\right)$, $Q'(t) = \mathrm{Im}\left(r'(t)\right)$, τ_{IQ} denoting the timing skew, ϕ_{IQ} the phase error, $g_{I,Q}$ and $o_{I,Q}$ the gain and offset of the I and Q components, respectively. Equation 3.1 gives important insights to how the signal is affected by such impairments. The effect of various in-balance impairments can be seen in Fig. 3.1 for the case of 16QAM. In (b), the effect of varying gain between $I(t)$ and $Q(t)$ results in signal compression of one of the axis relative to the other one. As a result, the effective power per dimension (considering constant average power) will vary, resulting in performance in-symmetry between I and Q. The effect of offsets (o_I,o_Q) is visualized (c) and we observe that while the constellation looks identical to the reference case in Fig. 3.1(a), the center of the constellation is shifted. Finally, a mis-match in the $\pi/2$ phase-shift between the two components causes the resulting vectors to be non-orthogonal which squeezes the constellation along the axis, as seen in Fig. 3.1(d).

Depending on the impairment, these in-balances can be compensated in different ways. Non-zero offsets can be compensated by re-centering the signal according to

$$r(t) = r'(t) - \mathbb{E}\left[r'(t)\right]. \tag{3.2}$$

Similarly, non-equal gain factors can be compensated for by scaling the signal according to

$$r(t) = k\left(\frac{I'(t)}{\mathbb{E}\left[|I'(t)|^2\right]}+j\frac{Q'(t)}{\mathbb{E}\left[|Q'(t)|^2\right]}\right), \tag{3.3}$$

with k being an arbitrary scaling constant. While gain variations and offsets might be straight forward to account for, a $\phi \neq 0$ causes the received in-phase and quadrature-phase components to be non-orthogonal. Several algorithms from basic linear algebra can be used to obtain orthogonal vectors, including the commonly used Gram-Schmidt (GS) orhogonalization scheme [88]. Using

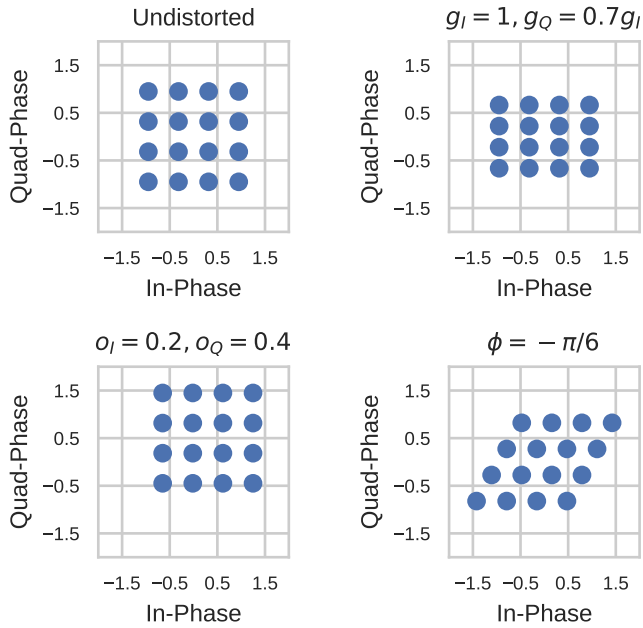

Fig. 3.1. Effect of IQ-inbalance on a signal constellation. (a) 16QAM reference case, (b) different gain of the I and Q component, (c) non-zero centered constellation in I and Q and (d) a $\phi = -\pi/6$ offset from the ideal case of a $\pi/2$ angular difference between I and Q component.

the GS scheme, one vector is selected as the reference and the second vector is then being orthonormalized with respect to the chosen initial vector according to

$$\begin{aligned} \vec{I}(t) &= \vec{I}'(t) \\ \vec{Q}(t) &= \vec{Q}'(t) - \frac{\left\langle \vec{I}'(t), \vec{Q}'(t) \right\rangle}{\left\langle \vec{I}'(t), \vec{I}'(t) \right\rangle} \vec{I}'(t), \end{aligned} \tag{3.4}$$

with $\vec{I}(t), \vec{Q}(t)$ being vectors in time and <> denoting the dot product. The effect of using the GS orthogonalization is depicted in Fig. 3.2. More importantly, according to Eq. 3.4, orthonormalization instead of orhogonalization

will compensate for any gain and offsets variations as well, requiring only a single step to compensate receiver IQ-imbalance.

As a final remark to the effect of in-balances it is important to note that while these algorithms work very well in idealized simulations, any noise on the constellations will be re-scaled when re-scaling the signal. Performance will therefore be limited in systems suffering from large in-balance. For the orthonormalization, several other methods exists which instead of normalizing one vector with respect to the other perform the orthogonalization in a symmetric way. In severe cases, such approaches can improve performance over the simple GS scheme.

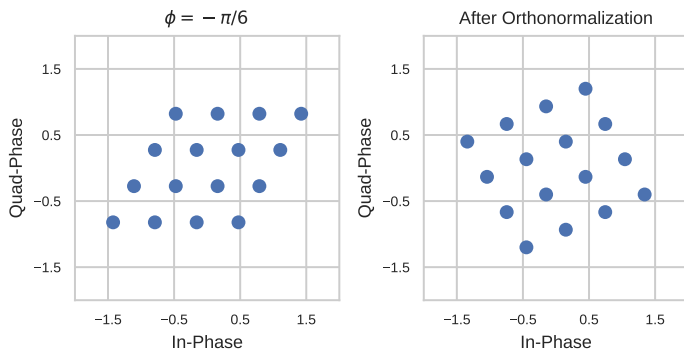

Fig. 3.2. Effect of orthonormalization to compensate for a $\phi \neq 0$. (a) before orthonormalization, $\phi = -\pi/6$. (b) after orthonormalization.

3.2 Static Equalization

Static equalization refers to the part of the DSP structure which compensates for static linear impairments such as dispersion [89]. While the distinction between static and dynamic filters is straight forward in theory, is is more fuzzy when considering the implementation of DSP-based filtering. This is due to the high flexibility of dynamic equalization (see Section 3.3) and several static impairments such as receiver bandwidth limitations are often handled by the dynamic equalizer, despite being of static nature. For the case of dispersion it is worth pointing out that the static assumption relies on a point-to-point link

with known, non-changing length. In dynamic network scenarios where optical signals are re-routed along the path, this might not be true and dispersion estimation is required to resolve the propagated distance [90]. However, this is still a slow process and in this work we focus on a fixed, known, transmission distance. Dispersion estimation has been extensively investigated for several different transmission scenarios and the interested reader is referred to [91–93].

3.2.1 Static Dispersion Compensation

A static dispersion compensation filter can be implemented by directly considering the frequency domain solution, Eq. 2.15, to the dispersive channel model (Eq. 2.12). Equalization can be implemented either using finite impulse response (FIR)-filters in the time domain or equivalently in the frequency domain [89]. Filtering using FIR-filters is covered in Section. 3.3. In principle, static frequency domain filtering could be implemented according to

$$r(t) = \mathscr{F}^{-1}\left(U(-z,\omega)\mathscr{F}\left(r'\right)\right), \tag{3.5}$$

with $\mathscr{F}$ denoting the Fourier transform operator and $U(z,\omega)$ is the dispersive phase response from Eq. 2.15. However, for real-time sequential processing it is necessary to apply the filter in a more continuous manner. This is done by dividing the signal into processing blocks from which each block is independently compensated by using a discrete Fourier transform implementation. To avoid issues from discontinuities and the periodic boundary conditions imposed by the use of block-wise Fourier transform [94]. To avoid this issue, the blocks are selected with a certain overlap which is then removed after processing, a process known as overlap and save [60, 95].

3.2.2 Matched Filtering

Matched filtering is the processes of maximizing the chances of detecting the signal correctly in the presence of AWGN by filtering it with a filter resulting in the least-mean-square error [61]. If a transmitter signal is shaped with a filter $h(t)$, the matched filter corresponds to the time-reversed complex-conjugate $h^*(-t)$. Matched filtering is a core part of communication theory and detailed derivations can be found in [61]. For the purpose of this thesis we only focus on the matched filtering criterion when using raised cosine (RC) pulse shaping for improving the spectral efficiency, as discussed in Section 2.1.2. When using a RC filter it is common to split the filtering between the transmitter and the

receiver. The transmitter filters the signal according to

$$s[n] = a[n] * h[n], \tag{3.6}$$

with $s[n]$ denoting the output discrete transmitted signal, $h[n]$ the transmitter pulse shaping filter and $*$ the convolution operator (Eq. 2.2). Assuming the AWGN channel, the received signal $r[n]$ can be written as (see Eq. 2.7 for a description of the AWGN channel model),

$$r'[n] = s[n] + N[n]. \tag{3.7}$$

To maximize the probability of correct detection, the receiver now uses the matched filter according to

$$r[n] = r'[n] * h^*[-n], \tag{3.8}$$

resulting in $r[n]$ being the least-mean-square estimate of the transmitted symbols $a[n]$. Important here is that when using RC pulses, is it often implemented by performing one filtering step at the transmitter and one at the receiver according to [61]

$$h_{\mathrm{RC}} = h_{\mathrm{Tx}} * h_{\mathrm{Rx}}. \tag{3.9}$$

In this case, the proper filter can be found by Fourier-transform Eq. 3.9 according to

$$H_{\mathrm{RC}}(\omega) = H_{\mathrm{Tx}}(\omega) H_{\mathrm{Rx}}(\omega) = |H(\omega)|^2, \tag{3.10}$$

which shows that the proper transmitter and receiver filters are the square-root of the overall sought response. Also note that while the key aspect of a RC filter is to shape the signal spectrum and ensure ISI-free operation, the ISI criterion is not full-filled by the square root RC filter (RRC) it self. Instead, ISI-free signaling is ensured by applying the matched receiver filter being implemented either by using the known filter response or via the use of a dynamic equalizer. Finally it is important to note that while being straight forward for the AWGN channel, matched filtering is more tricky for a more general fiber-optic channel and careful DSP design is needed in order to minimize ISI. Similar to the case of dispersion compensation, matched filtering can be implemented either in the time or in the frequency domain.

3.3 Dynamic Equalization

Some effects present in optical communication systems are not static and requires dynamic tracking or dynamic equalization. Moreover, residual dispersion or miss-matches in the static filtering can be compensated for by dynamic

tracking which ensures that the overall receiver filter response is the one which maximize the probability of correct detection [89].

Similarly as for the case of static equalization outlined in Sec. 3.2, dynamic filtering can be implemented in the time or frequency domain. To give the complete picture, the following description uses the time domain implementation. Which one to choose depends largely on the memory length of the filter as computations of long responses can be done more effectively in frequency domain. This is of key importance for SDM systems with long impulse responses such as mode-division multiplexing systems [96, 97].

FIR filtering can be described as

$$r[n] = \vec{h}^*[n] \cdot \vec{r'}[n], \tag{3.11}$$

with $\vec{h} = [h(n),h(n-1),...,h(n-N)]$ and similarly for the received signal prior to equalization $\vec{r'}$. Here N is the memory length of the filter. Also note that the filter can be shifted to have memory both forward and backwards in time which is required for matched filtering of, for example, RC pulses. However, doing so always introduces a fundamental delay of the filter, to maintain causality.

In the case of dual-polarization transmission, the equalizer can be used to undo polarization rotations and compensate for PMD. To do this, the equalizer needs to be expanded to account for both polarization. This is done using 2×2-butterfly configuration of the equalizer according to [60]

$$\begin{pmatrix} r_X[n] \\ r_Y[n] \end{pmatrix} = \begin{pmatrix} h_{XX}[n] & h_{XY}[n] \\ h_{YX}[n] & h_{YY}[n] \end{pmatrix} \begin{pmatrix} r'_X[n] \\ r'_Y[n] \end{pmatrix}. \tag{3.12}$$

In contrast to the previously outlined single dimension equalization, Eq. 3.12 implements the polarization de-multiplexing required in dual-polarization systems. Important here is that pure polarization rotations can be undone using a 2×2 complex unitary matrix and no time memory is needed. Instead, the memory requirement in the polarization de-multiplexing process arises due to the PMD present in optical fibers and the requirement of ensuring match filtering.

In order to perform dynamic equalization, the filtering elements in Eq. 3.12 has to be dynamically updated. Considering one update step, the tap update

can be done using stochastic gradient decent according to [98]

$$\begin{aligned} h_{XX}[n+1] &= h_{XX} + \mu\epsilon_X[n]r_X^*[n]r'_X[n] \\ h_{XY}[n+1] &= h_{XY} + \mu\epsilon_X[n]r_X^*[n]r'_Y[n] \\ h_{YX}[n+1] &= h_{YX} + \mu\epsilon_Y[n]r_Y^*[n]r'_X[n] \\ h_{YY}[n+1] &= h_{YY} + \mu\epsilon_Y[n]r_Y^*[n]r'_Y[n] \end{aligned}, \tag{3.13}$$

with $\epsilon_{X/Y}$ denoting the error function and μ being a constant (error scaling factor) known as the step length. Several different error functions exists of which some are covered in the following sections. A more detailed overview over different algorithms can be found in [60, 99]. The power of dynamic equalization can be seen in Fig. 3.3, in which the dynamic equalizer is used for both polarization de-multiplexing and matched filtering on the receiver side.

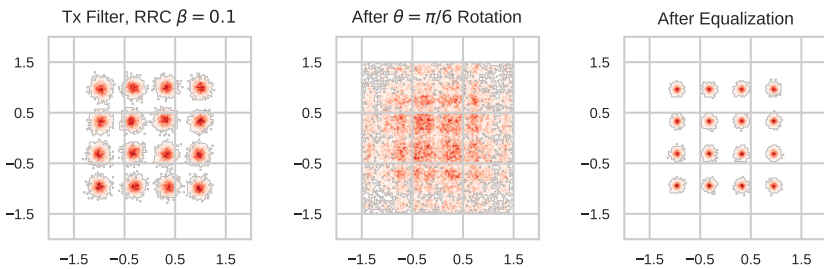

Fig. 3.3. Effect of dynamic equalization. (a) Transmitted signal shaped with a root-raised cosine filter with $\beta = 0.1$. (b) resulting constellation after a small polarization rotation. (c) Constellation after dynamic equalization.

3.3.1 Constant Modulus Algorithm

The constant modulus algorithm (CMA) is one of the key algorithms in dynamic equalization [100]. The CMA is based on minimization of the mean squared error of the signal, with respect to a given reference level, R_{Ref}, according to [100, 101]

$$\begin{aligned} \epsilon_{\text{X}} &= R_{\text{Ref}} - |r_{\text{X}}[n]|^2 \\ \epsilon_{\text{Y}} &= R_{\text{Ref}} - |r_{\text{Y}}[n]|^2 \end{aligned}. \tag{3.14}$$

The CMA is a simple, frequently used, very powerful error function. However, as seen in Eq. 3.14, the average power is always referenced with respect to a

fixed value. For constant power constellations such as QPSK, this is optimal but for multi-level modulation formats such as general M-QAM this is not true. Still, by choosing R_{Ref} according to [102]

$$R_{\mathrm{Ref}} = \frac{\mathbb{E}\left[|a[n]|^4\right]}{\mathbb{E}\left[|a[n]|^2\right]}, \tag{3.15}$$

the standard CMA can be used for multi-level modulation formats at the expense of a penalty, which becomes larger when increasing the modulation order.

3.3.2 Radius-Direct Equalization

Focusing on multi-level modulation, one way of extending the CMA is to use a radius-directed equalizer (RDE) [103]. As given away by the name, this equalizer relies on estimating the radius of the equalizer output and compare it to a set of reference levels (in contrast to CMA which only has one fixed level). This is done by adapting Eq. 3.14 according to [103]

$$\begin{aligned} \epsilon_{\mathrm{X}} &= \mathbb{D}\left[|r_{\mathrm{X}}[n]|^2\right] - |r_{\mathrm{X}}[n]|^2 \\ \epsilon_{\mathrm{Y}} &= \mathbb{D}\left[|r_{\mathrm{Y}}[n]|^2\right] - |r_{\mathrm{Y}}[n]|^2 \end{aligned}, \tag{3.16}$$

with $\mathbb{D}$ denoting a radius decision operator which selects the maximum-likelyhood radius of the received constellation point given a set of reference radii. As such, the use of RDE requires knowledge of the constellation. Moreover, the performance depends on the probability of correctly estimating the signal radius. This is even more challenging during the initial convergence phase in which symbol errors are frequent. To overcome this, a RDE is often used in cascade with an initial CMA equalizer to pre-converge the taps. After the CMA has converged to the best average error, the RDE is used to account for the multi-level constellation.

3.3.3 Decision-Directed Least Mean Square

The RDE can be seen as an extended CMA which uses a decision-directed (DD) circuit to choose the most proper reference level from a given reference set, resulting in a real-valued error signal. Instead, a decision on the most likely received symbol can be used and the error taken as the distance between the received symbol according to [104, 105]

$$\begin{aligned} \epsilon_{\mathrm{X}} &= \mathbb{D}\left[r_{\mathrm{X}}[n]\right] - r_{\mathrm{X}}[n] \\ \epsilon_{\mathrm{Y}} &= \mathbb{D}\left[r_{\mathrm{Y}}[n]\right] - r_{\mathrm{Y}}[n] \end{aligned}, \tag{3.17}$$

refereed to as DD least mean square (DD-LMS) equalizer with $\mathbb{D}$ now denoting the symbol decision operator . The use of a DD-LMS is suitable for complex multi-level constellations such as higher-order M-QAM. In contrast to CMA and RDE, the DD error function uses both the real and imaginary part of the signal error. If carrier offsets (see Section 3.4) are present on the signal, these have to be compensated in order to make accurate symbol-based decision which causes delays in feedback when considering real-time processing. Moreover, similar to RDE, the DD-LMS is sensitive to symbol decision and initial pre-convergence is normally required to ensure stable performance.

3.4 Carrier Recovery

In addition to the powerful static and dynamic equalization used to compensate for linear transmission impairments, any miss-match between the transmitter and receiver laser will give raise to carrier offsets [106]. This can be qualitatively understood by considering the up-down conversion process done in the transmitter and receiver according to

$$r[n] = a[n] \exp\left(j\left(2\pi n T_0 f_0 + \phi_0[n]\right)\right) \cdot \exp\left(-j\left(2\pi n T_0 f_1 + \phi_1[n]\right)\right) + N[n], \tag{3.18}$$

with f_0,f_1 and ϕ_0,ϕ_1 denoting frequency and phase noise of the transmitter and receiver lasers, respectively and T_0 denoting the symbol duration. Ideally, the transmitter and receiver laser are perfectly synchronized and without any phase noise. However, in practise the lasers drift and have a finite linewidth (the ideal laser is monochromatic). How much and to what extent depends on the laser type but for standard external cavity lasers (ECLs) used in the majority of this work, frequency drifts up to a few GHz together with linewidths around 10-100 kHz are common.

While the dynamics underlying the linewidth of a laser can be complex, an easy system model can be built up under the assumption of a perfectly Lorentian linewidth. In such case, the phase noise can be approximated as a Brownian motion according to [106]

$$\phi[n] = \sum_{k=-\infty}^{n} \nu[k], \tag{3.19}$$

with $\nu[k]$ being *i.i.d.* Gaussian random variables with zero mean and variance $\sigma_\nu^2 = 2\pi\Delta\nu T_0$, with $\Delta\nu$ being the laser linewidth (often combined for both the transmitter and the receiver laser). In contrast to frequency offset which

corresponds to a linear phase walk, phase noise is a random process. Moreover, the frequency offset is a slow varying process in contrast to phase-noise compensation which is required on symbol level to ensure high performance.

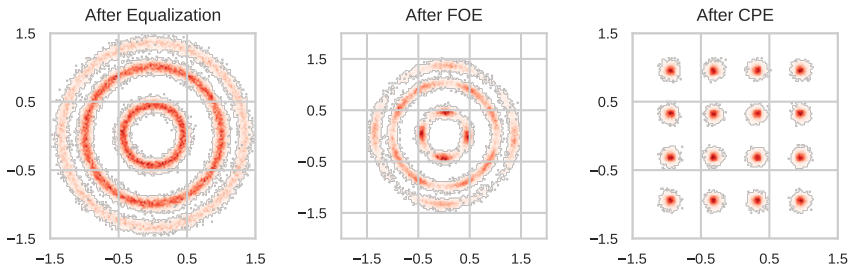

Fig. 3.4. Impact of DSP-based carrier recovery. (a) shows signal before compensation, $\Delta f = 500\text{MHz}$, $\Delta\nu = 100\,\text{kHz}$. (b) constellation after FOE and (c) constellation after FOE + CPE (BPS with $M = 64$ and $N = 20$).

3.4.1 Frequency Offset Estimation

DSP-based frequency offset estimation (FOE) can be done in several ways [107–112]. While most studies have been considering offline processing, some recent work has focused on hardware implementations of FOE [113]. One commonly used approach is the based on trying to remove the data modulation and then estimating the frequency offset by finding the linear component of the signal phase drift. This can be understood by considering QPSK modulation for with the symbols $a[n] \in \frac{1}{\sqrt{2}}(\pm 1 \pm j)$. QPSK is equivalent to 4-phase shift keying (PSK) and for M-PSK formats, data modulation can be removed by raising the constellation to the M:th power [106]. In the case of QPSK, this translates to

$$(a[n])^4 = -1, \forall n. \tag{3.20}$$

Similar expression holds for all M-PSK. After this process, the frequency offset is found using a linear fit of the phase trace in the time domain, or by Fourier transforming the signal and search for the maximum peak in the resulting spectrum (which is intuitive since the Fourier-transform is nothing else than a change of basis to a set of linear orthogonal frequency components) [112].

While proven powerful for M-PSK, the expression in Eq. 3.20 cannot be generalized to an arbitrary QAM format and there is no trivial operation

which simply removes the data modulation (which follows from the fact that in contrast to PSK, both the amplitude and phase are used for encoding information). However, for M-QAM, this can usually be circumvented by realizing that M-QAM constellation can be decomposed to rings of PSK. For example, a 16-QAM can be decomposed into an inner and an outer ring with QPSK and an intermediate with 8-PSK. Since they have different power, applying Eq. 3.20 to such a constellation will map to 4 points, from which 2 are mapped to the real axis (but with different amplitude). Doing so, the same algorithm can be used even for higher order M-QAM at the expense of requiring more symbols as only a fraction of the symbols actually directly are used to estimate the frequency offset. This can be seen in Fig. 3.4 for the case of 16QAM and 64QAM together with the reference case of QPSK.

As a final remark, while long averaging filters are not an issue in offline processing, they are for real-time implementations. Moreover, the accuracy of the estimation depends on the number of symbols used. As a result, the complexity of frequency offset estimation grows when considering systems operating at low received SNR with a strong presence of symbol errors.

3.4.2 Carrier Phase Estimation

The role of the carrier phase recovery (CPE) is to compensate the random walk caused by the phase-noise. In addition, it also compensates for any residual frequency offset due to limited resolution of the frequency offset estimation, a very important aspect which is often overlooked in simulation work. For PSK-signals, the carrier phase recovery can be implemented the same way as the frequency offset estimation by raising the signal to the M:th power, in line with Eq. 3.20. However, instead of doing a linear fit over a large set of symbols, a sliding average window is used to track and follow the phase fluctuations [114]. This is referred to as Viterbi-Viterbi (VV) phase estimation [115]. In such case, the relation between the amount of phase noise and AWGN decides the optimal block length.

As pointed out in Section 3.4.1, the data modulation can be removed in an optimal for M-PSK but modifications are required to allow processing of arbitrary M-QAM. This is often done by considering partitioning the constellation into several PSK rings [114, 116–118]. A frequently used alternative to Viterbi-based CPE for arbitrary M-QAM is the blind phase search (BPS). In contrast to Viterbi-based CPE which relies on a nonlinear operator to remove data modulation, BPS relies on parallel processing using a brute-force scheme

in which a set of M test angles are selected according to [119]

$$\phi_m = \frac{m}{M}\frac{\pi}{2}. \tag{3.21}$$

The received symbols are then rotated with every test phase before a decision operator is used to calculate the distance error according to

$$|d_{n,m}|^2 = |r'[n]\exp(j\phi_m) - \mathbb{D}\left(r'[n]\exp(j\phi_m)\right)|^2, \tag{3.22}$$

before a sliding average window of length $2N+1$ is used to suppress noise according to

$$s_{n,m} = \sum_{k=-N}^{N} |d_{k,m}|^2, \tag{3.23}$$

and the output symbol is then selected by minimizing $s_{n,m}$ over the M test angles according to

$$r[n] = \arg\min_m s_{n,m}. \tag{3.24}$$

Following its parallel nature and compatibility with arbitrary M-QAM modulation formats (due to the symbol-based decision in Eq. 3.23), BPS is often used for processing higher-order M-QAM formats. Extensions with maximum-likely hood estimators to improve robustness have also been studied using a two-stage approach [120]. Worth noting here is that the needed number of test angles, M, and averaging block length, N, depends on the modulation order and amount of AWGN present. As a result, processing of higher-order formats in a regime with low SNR can be challenging. Since the CPE also has to cover any remaining frequency offset, which also is more likely in this regime of interest, extra care is required when designing carrier recovery for high spectral efficiency systems using strong FEC. This issue is discussed in Paper C.

3.5 Compensation of Transmitter Distortions

Following the CPE, the output symbols are usually fed to a de-mapper followed by a decoder to recover the bits. However, similar to how an initial IQ-imbalance compensation stage can be used to compensate for receiver IQ-imbalance, additional compensation can be used to compensate for transmitter distortions [86, 93]. These distortions are the same as the once outlined in Sec. 3.1 for the case of the receiver and can be compensated in the same way. For a well-balanced transmitter, this stage is usually not needed and in the case of minor distortions a single orthogonalization stage is usually sufficient. However,

for completeness, it is important to point out that real-valued equalization can be used to combat more severe distortions and improve performance. This is typically needed in systems with subcarrier-modulation [85]. The key difference is while a complex modulation assume orthogonality between I and Q, a real-valued can be used to compensate for scenarios when this is not the case [121].

3.6 Pilot-Based DSP

In contrast to previously outlined blind algorithms relying on signal statistics or estimations of transmitted symbols such as DD-approaches, pilot-based DSP relies on a set of transmitted symbols which are known to the receiver [99]. This makes pilot-based DSP highly flexible and very powerful, especially for higher-order modulation formats which are very sensitive and hard to processes using blind DSP [122]. Pilot-based DSP is also considered for flex-format transceivers as the DSP is transparent to the used modulation format [123, 124].

A more detailed discussion on the power and implementation of pilot-based DSP is left for the future. Key aspects of pilot-based DSP includes design and overhead minimization to combat rate-loss from pilot transmission. While pilot-based DSP approaches are often considered sub-optimal in the research community, the are inherent very robust and powerful, making them suitable for usage in "real" systems [122].

However, it is worth to point out that several recent experiment have been using data-aided (DA) equalization to improve performance [99]. While often used in experimental work, this is a non-practical approach requiring full knowledge of the transmitted pattern and it should therefore belong to the category of pilot-based approaches. While seldom discussed, overhead of DA-approaches should also be considered when estimating performance of systems.

3.7 De-Mapping and System Performance Evaluation

After carrier recovery and compensation of transmitter distortions, the next step is to de-map the transmitted symbols to a bit stream which then is forwarded to the FEC decoder used to recover the transmitted bits. Important to note here (and all to often overlooked in the experimental literature) is that several types of codes exist and depending on the chosen type, the output from

the de-mapper can be either soft or hard. While coding is seldom implemented in transmission experiments and other performance metrics are used instead, distinction between hard and soft codes is necessary as they require different metrics to accurately predict the performance after decoding.

3.7.1 Hard-Decision Demapping

The classical de-mapper is a hard decision (HD) de-mapper which outputs the maximum likelihood bit sequence given the received symbols. Assuming the AWGN channel (this assumption is most often used when designing de-mappers), this corresponds to selecting the closest constellation symbol to the transmitted ones.

The implication of the assumption of a HD-FEC is that measured BER after the de-mapper can be used to verify that the system performs within the target limit of a code assumption which usually is around BER $\approx 1 - 5 \cdot 10^{-3}$ with corresponding coding overheads of around 7% .

3.7.2 Soft-Decision De-mapping

Recently, more and more research has turned towards studying the use of soft-decision (SD) FEC which is capable of improved coding gain at the expense of increased complexity of the de-mapper and the de-coder. Code-design and structures are far beyond the scope of this thesis, and we therefore only focus on performance metrics used to estimate the performance.

The first key difference between HD- and SD-decoding is that instead of forwarding de-mapped bits, a SD-demapper outputs log-likelihood ratios (LLRs) which can be understood as the probability of that bit being a 1 or a 0. The corresponding case of HD would be to simply output the most likely outcome of the corresponding bit. For a complex symbol there exits $k = \log_2 M$ LLRs as [125]

$$L[k] = \log \frac{\sum_{x \in \chi_k^1} P_{X|C_k}(x|1) f_{Y|X}(y|x)}{\sum_{x \in \chi_k^0} P_{X|C_k}(x|0) f_{Y|X}(y|x)}, \tag{3.25}$$

with χ_b^b is the set of constellation symbols with $b \in 0{,}1$ at bit position $k \in 1{,}..., \log_2 M$ and $f_{Y|X}(y|x)$ is the probability of a received symbol Y conditioned on a transmitted symbol X. After calculating the LLRs, these values are forwarded to the FEC decoder. The improvement of using LLRs can easily be understood by considering a sequence of bits in which one is wrong (as detected by the parity check in the decoder). If only the bits are present, all

bits are equally likely to be the one being wrong (even though clever encoding and decoding algorithms allows for educated guesses) but if the LLRs are present, statistical knowledge of the probabilities of each bit being wrong are available and the most uncertain one can be changed. However, the price of SD comes at the higher computational complexity in both the de-mapper and the decoder.

Estimating the performance of a system with soft-decision is a bit more tricky and requires assumptions on which SD code being used. Assuming a memory-less channel and the use of bit-interleaved coded modulation (BICM), the proper metric to use is the generalized mutual information (GMI) [125]. If one instead allows for the use of non-binary codes or iterative de-mapping, the proper metric is the mutual information (MI) [125]. Also note that the GMI is upper bounded by the MI. Assuming a memory-less AWGN channel, the GMI can be estimated according to [125, 126]

$$\mathrm{GMI} \approx M - \frac{1}{n_s} \sum_{k=1}^{M} \sum_{l=1}^{n_s} \log_2 \left(1 + \exp\left((-1)^{c_{k,l}} \lambda_{k,l}\right)\right), \tag{3.26}$$

using a sequence of $M \cdot n_s$ transmitted bits denoted by $c_{k,l}$ and the corresponding L-values $\lambda_{k,l}$ estimated using Eq. 3.25. A comparison between BER and GMI for standard M-QAM modulation formats in the AWGN channel can be seen in Fig. 3.5.

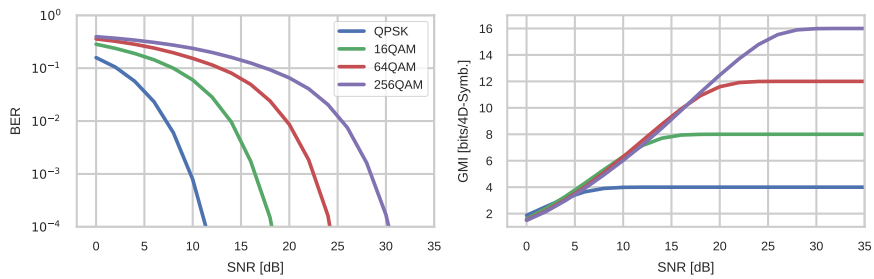

Fig. 3.5. Comparison between BER and GMI for standard M-QAM modulation formats in the AWGN channel. (a) bit error ratio (BER) and (b) generalized mutal information (GMI).

Two additional considerations are important when discussing performance metrics and codes. The first is that good channel models to estimate the statics of a received symbol given a transmitted one are lacking for transmission in

the optical fiber. Instead, mapping schemes and codes are often designed under the assumption of a memory-less AWGN channel and deviations from ideal performance can therefore be expected. However, with uncompensated transmission around optimal launch power, the AWGN is in general a good model. Secondly, the purpose of the FEC is to ensure a residual BER below a given level, usually selected as 10^{-15}. Powerful SD-codes such as the frequently used low-density parity-check (LDPC) codes have an error floor which usually is significantly above the target value and also not possible, to date, to predict fully from analytically estimates. To ensure that the target performance is met, the SD code is usually concatenated with an outer HD-FEC. The combination of these two codes ensures target performance, not simply switching from a HD-FEC to a SD-FEC. Coding is a research field by itself and from the perspective of this thesis we therefore simply measure use the performance metrics and assume that the code can be implemented. For combinations of SD and HD codes, see [26, 56, 125].

Chapter 4

Frequency Combs in Fiber-Optic Communication

This chapter describes WDM transmission and how frequency combs can be be used in WDM systems. Frequency combs are first introduced before specific applications in optical communication are discussed. Finally, we discuss the basis for the comb-based superchannels using shared pilot tones presented in Paper A-D.

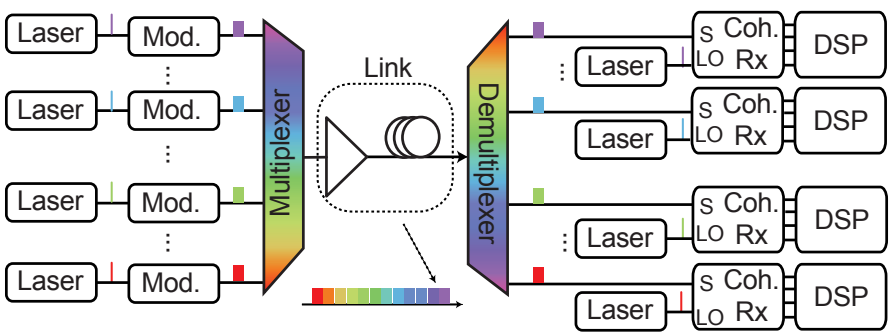

Fig. 4.1. Principle of a standard multi-channel WDM system. Each channel consists of an optical transceiver, operated independently from all other co-propagating channels.

4.1 Wavelength Division Multiplexing

The concept of WDM has been introduced in Section 1 and it plays a key role in enabling the massive throughput from optical links by making use of the SMF bandwidth spanning about 10 THz (only considering the C+L-band) [38, 49]. The principle for a WDM system is shown in Fig. 4.1 and can be understood by considering several single-channel systems, each one following the principle outlined in Section 2. To fill the full bandwidth, each wavelength channel is chosen so that all channels are separated in the frequency domain. At the receiver, the target channel is selected by filtering out the side channels and matching the LO to the transmitter laser wavelength.

4.2 Frequency Combs

An optical frequency comb is a coherent multi-wavelength light-source characterized by its center frequency f_0 and its line spacing Δf, as shown in Fig. 4.2. While these two parameters characterize a frequency comb [127], several different ways of generating one exists. These include the use of mode-locked lasers [128], four-wave mixing in micro-ring resonators [129] and optical fibers [130] and electro-optic modulation [127]. Optical frequency combs have been used in spectroscopy [131, 132], optical arbitrary waveform generation [133], optical frequency synthesizing [134] and in communications [127]. In 2005, John L. Hall and Theodor W. Hänsch were awarded the Nobel prize in physics "for their contributions to the development of laser-based precision spectroscopy, including the optical frequency comb technique", highlighting the impact of comb technology as a scientific tool.

Throughout this thesis, electro-optic (EO) frequency combs are used. Here, an EO comb is generated using a cascade of over-driven phase modulators (PMs) and intensity modulators (IMs) [135]. The setup for generating an EO-comb is shown in Fig. 4.3 together with the resulting spectrum of an EO-comb consisting of two PMs and an IM. All modulators are driven by a common radio-frequency (RF) clock, setting the line spacing Δf. To generate the about 50 lines from the comb, two high-power RF amplifiers are used before the PMs. The intensity modulator acts as a pulse carver with 50% duty-cycle, which if correctly biased, carves the pulses only when the PM provides an almost linear chirp [127, 136]. If the RF-phase shifts shown in Fig. 4.3 are correctly aligned, the output spectrum is very flat with two characteristic "ears", as shown in Fig. 4.3. The center frequency f_0 is set by the comb seed lasers and EO-combs are hence fully characterized by the RF-clock and the

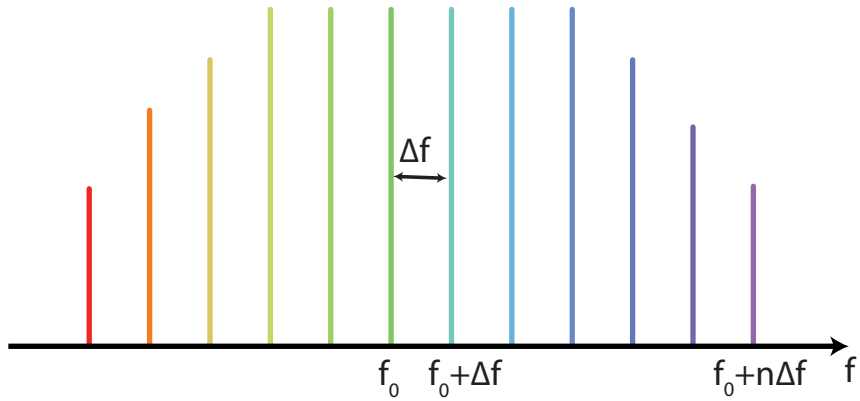

Fig. 4.2. Principle of an optical frequency comb. The comb can be fully characterized by its center frequency f_0 and its line spacing Δf.

seed laser. Using high-power handling modulators, EO-combs can be very stable and produce lines with high line power.

4.3 Comb-Based Transmission Systems

Studying the WDM system shown in Fig. 4.1, one can intuitively understand how frequency combs can play a role in future WDM systems. Since all wavelength channels are separated by a given spacing (which often is fixed to one of the defined ITU grids), a single multi-wavelength source could, in principle, be used instead of the N lasers used on the transmitter and receiver side. The principle of an optical communication system using frequency combs is shown in Fig. 4.4. Here, all transmitter laser and LOs are replaced with a transmitter and a receiver frequency comb. Since the carriers of a frequency comb are locked with respect to each other, all channels are locked on the grid provided by the frequency combs line spacing Δf. To date there have been several demonstrations of comb-based transmission systems using a broad range of comb sources. These include the use of combs based on the Kerr effect in micro-ring resonators (MRR) [129], mode-locked lasers [137], electro-optic (EO) modulation [138] and parametric broadening optical fibers [139]. Several recent demonstrations have shown promising results for integrated multi-wavelength sources using MRR-generated combs

as a light source. These include the first demonstration of transmission using using a low-noise MRR-based comb at distances reaching 300 km [140], dense WDM transmission using two interleaved combs [129], the use of MRR-based combs both in the transmitter and receiver [129], communication over trance-oceanic distances [141] and compatibility with higher-order modulation formats by demonstrating transmission with PM-64QAM [142]. Mode-locked lasers have long been considered for use in optical communication [137, 143] and recent advantages using external cavities demonstrated compatibility with PM-32QAM, overcoming classical linewidth issues using mode-locked lasers [144]. Dense WDM transmission using EO-combs was investigated in [145]. They are also the based of the parametric combs in [139] in which an EO-comb is used to generate an initial comb from which two (or a few) lines are selected and send through a parametric mixer used to create ultra-flat combs exceeding 100 nm BW [130, 139]. The minimum carrier OSNR of such parametric combs can exceed 45 dB with minimum line power exceeding 5 dBm [146], enabling record demonstration of 2.15 Pb/s throughput over a 22-core fiber [147]. The high OSNR has also enabled transmission of PM-256QAM [148].

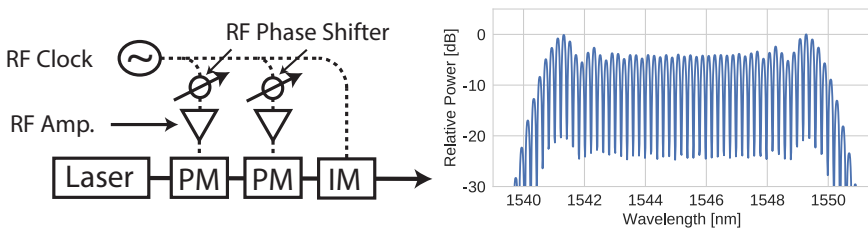

Fig. 4.3. EO-comb generation setup together with the resulting spectrum measured using 0.1 nm resolution.

4.4 Exploiting Unique Comb Properties in Coherent Optical Communications

The combined research efforts have been successful in validating the possibility of using frequency combs as a WDM source in optical communication. Depending on the target application, various comb technologies (mentioned in Section 4.3) have proved to meet the demands, potentially replacing the use of independent free-running lasers in WDM applications. Simply replacing free-running laser has the potential of enabling energy savings [129, 142].

Beyond the simple case of replacing free-running lasers with a multi-wavelength source, much less effort have been put into actually exploiting the unique properties brought by introducing frequency combs. Pioneering work on this was done in [149] where the authors demonstrated two-folded reach-increase by using transmitter-side digital pre-compensation of fiber non-linearities. This compensation was enabled by exploiting the property of frequency locked carriers from an optical comb and the benefit of the scheme would be lower if implemented with free-running lasers [150]. Another example of DSP-based concept exploiting unique comb properties includes joint CPE to reduce DSP power consumption [151] but lots of work remains before the role of frequency combs is fully understood.

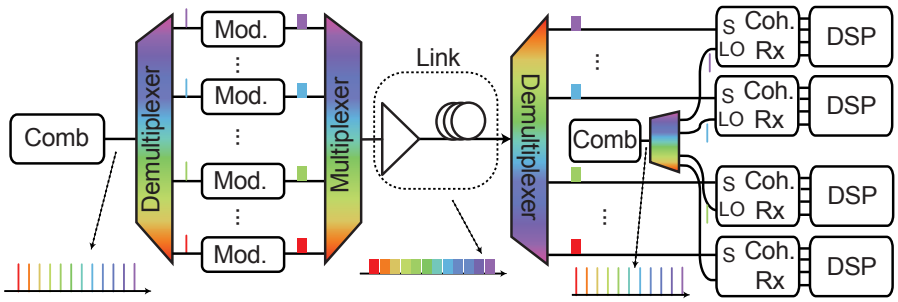

Fig. 4.4. Illustration of a comb-based WDM system. All channels originates from a common comb-source and the receiver LO lines are generated from a receiver combs. Modulation and receiver processing is typically done independent for each wavelength channel.

4.4.1 Self-Homodyne Detection

In early days of coherent optical communication, self-homodyne (SH) detection was proposed as a way of combating the laser phase noise and avoid the need for complex DSP-based carrier recovery (as described in Section 3.4.2) [152]. Instead of using a free-running laser as LO, a copy of the transmitter laser is transmitted as a pilot tone (PT) and used as LO. This avoids the need for FOE and, in the ideal case, completely removes any laser phase noise. Conventionally, the orthogonal polarization is used for PT transmission implying a 50% loss in SE. In addition, the PT is subjected to noise and nonlinear impairments from propagation (see Section 2.2.3). SNR dependence of PT filtering was investigated in [153] and capabilities for SH systems to cancel out nonlinear

signal distortions was demonstrated in [154]. Despite the clear advantages of reduced DSP complexity, the loss in SE battled SH systems and to combat this, interleaved PT transmission was proposed, reducing the overhead to 33% [155].

More recently, SH detection was expanded into the domain of SDM transmission. The many spatial dimensions available allows for effecting sharing of a pilot tone by using the high correlation among separate cores within a multi-core fiber [156]. This was demonstrated in [157] where the authors used a 19 core fiber with one core dedicated for PT transmission. The capabilities of the scheme were later used in a high throughput experiment demonstrating 210 Tb/s throughput using high-linewidth laser by combining the SH detection with WDM [158]. Cross-talk dependence and correlations within multi-core fiber were investigated more in-depth in [159].

4.4.2 Frequency Comb Regeneration

While exploiting the high correlation of spatial dimensions using SDM fiber provided SH detection with low overhead, the number of WDM channel still exceeds the number of available SDM channels, even in record experiments combining both multi-mode and multi-core transmission [50]. Moreover, as the number of wavelength channels is very high in fully loaded systems, the complexity is still high if using one PT per wavelength channel. As briefly outlined in Section 4.3, frequency combs provides high correlation among channels in the spectral domain. Comb-based superchannels can therefore be treated in similar ways to spatial superchannels. This implies that gains and sharing can be exploited also in SMF technology, making comb-based superchannels compatible with existing infra structure.

The idea of exploiting the coherence was first proposed in [143] where the authors proposed locking of a transmitter and receiver comb using two unmodulated PTs. The first system study of properties for a comb-based SH system was done in [160]. The experiment was done in back-to-back and the authors only considered recovering the central tone of the frequency comb, or equivalently, locking f_0 of the two frequency combs. As only one tone was used, the same RF-clock reference Δf was used in both the transmitter and the receiver to enable full phase coherence. This issue was solved in [161] which studied the use of two PTs, enabling recovery of both f_0 and Δf, creating a fully self-homodyne system. The effects of dispersive walk-off between the PTs (similar to skews in the case of multi-core fiber) were highlighted and experimentally verified [161]. The first transmission using frequency comb regeneration for self-homodyne detection was done in [162], demonstrating transmission of a 24×20 Gbaud PM-32QAM superchannel using Brillouin

amplification to provide narrow optical filtering and avoid excessive phase noise on the regenerated comb.

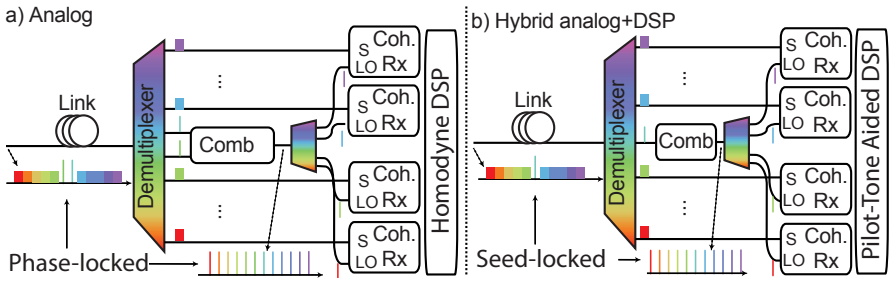

Fig. 4.5. Comparing comb regeneration using one and two pilot tones. (a) two pilot tones are used to lock both f_0 and Δf between the transmitter comb, providing a fully SH system which eliminates the requirement of DSP-based carrier recovery. (b) a single pilot tone is used to lock f_0 while Δf is left without synchronization. However, the comb stability is order of magnitude better than the stability of the seed lasers (assuming standard lasers) and the residual offsets can easily be tracked using DSP.

To avoid penalties from the line-width scaling reported in [162], Paper A demonstrated regeneration using a receiver EO frequency comb. While the Brillouin amplifiers used in [162] provided filtering BW around 20 MHz, Paper A introduced the use of an electrical phase-locked loop (PLL) to provide orders of magnitude more narrow filtering. As a result of this, regeneration can be performed with higher quality. This enabled both a doubling of the number of regenerated lines as well as an increase in modulation format from PM-32QAM to PM-64QAM, resulting in a combined superchannel throughput of 10 Tb/s with a spectral overhead of 4% for self-homodyne detection.

The requirement of using two tones can be understood by considering the the setup for generating an EO-comb, as shown in Fig. 4.3. One PT is sufficient to directly extract the center frequency and the beating between two neighboring tones gives the spacing Δf. However, in the case of EO-combs, carrier offsets caused by non-ideal synchronization of f_0 and Δf result in very different impairments. Not locking the central carrier f_0 simply creates an intradyne system, similar to the ones described in Section 2, requiring DSP-based carrier recovery as outlined in Section 3.4. If f_0 is locked but not Δf, the requirements for DSP-based carrier recovery are dictated by the clock (comb) stability instead of the comb seed lasers. While impairments from not knowing Δf also will result in additional frequency offset and phase

noise, RF-clocks are orders of magnitude more stable compared to standard free-running lasers.

As a result of this, the effective gain from going from intradyne to a single PT is much larger than going from one to two PTs, considering both DSP complexity and performance gain. A single PT used to lock f_0 removes the need for FOE and, depending on laser quality and patch-matching, suppresses phase noise. At the same time, a single pilot tone is robust to nonlinear distortions and avoids the additional complexity of using phase-locked loops to lock spacing. Details of the single PT concept and its implications can be found in Paper B-D.

Chapter 5

Conclusions and Future Outlook

The coherence of frequency combs provides unique possibilities for joint processing to improve performance and relax the complexity of the receiver, while still maintaining high spectral efficiency. This thesis is centered around comb-based superchannels and their potential application in systems using wavelength-division multiplexing. However, in contrast to classical system using independent processing for each wavelength channel, the transmitter and receiver comb are synchronized via the use of optical pilot tones. The synchronization enables effective cancellation and/or suppression of carrier offsets, reducing the receiver requirements. If two pilot tones are used, the transmitter and receiver comb can be fully phase-locked, enabling operation using higher-order modulation formats without requiring any carrier recovery using digital signal processing. This was demonstrated in Paper A, enabling self-homodyne detection of a 50×20 Gbaud PM-64QAM superchannel with 4% spectral overhead.

While two pilot tones are needed for full phase locking, carrier offsets can be divided between offset from the comb seed lasers and offsets from the comb sources. A single pilot tone is enough to synchronize the transmitter and receiver comb seed lasers, removing frequency offset and suppressing phase noise while adding minimal complexity. This hybrid approach of combining a single optical pilot tone with digital carrier recovery facilitates the use of blind processing, enabling processing of higher-order modulation formats with standard algorithms. This was demonstrated in Paper B by transmitting

a 54×24 Gbaud PM-128QAM superchannel reaching a spectral efficiency of 10.3 bits/s/Hz. The scheme was furthermore proved tolerant to transmission impairments, enabling effective usage of pilot tones for transmission distances reaching 1000 km as shown in Paper C. The minimal overhead furthermore enabled record-high spectral efficiency of 11.5 bits/s/Hz for fully loaded C-band transmission, as demonstrated in Paper D.

These combined results show that optical pilot tones can be used in high spectral efficiency transmission systems thanks to the effective sharing enabled by the use of coherent frequency combs. Moreover, synchronizing transmitter and receiver combs fully in the optical domain allows for exploiting the gain without requiring any joint processing in the digital domain. The proposed schemes therefore provides flexibility and compatibility with standard algorithms but with less stringent requirements. This enables a new degree of freedom when designing and optimizing superchannels for high spectral efficiency transmission while striving to maintain low complexity.

Based on these results, several interesting topics can be considered for future studies. This includes investigations of analog and digital pilot as well as combinations of both. While the optical pilot tones provides effective suppression of carrier offsets, digital pilot symbols provides a large degree of flexibility in design, making combinations of both interesting to study from a performance-complexity viewpoint.

Other interesting applications for superchannels lies in the domain of SDM and superchannels spanning both spectral and spatial domain can enable new degrees of freedom when optimizing overhead. In such applications, balance between limitations from spatial skew and comb phase noise are likely to affect the design. It also opens the possibility for multi-dimensional modulation and coding applied over the massive signal space spanned by the spectral-spatial superchannel. Depending on the distortion level and its distribution in frequency and space, optimization can be done to minimize the overall overhead by making use of available processing resources, being either analog, digital or both, in the most effective way.

Chapter 6

Summary of Papers

Paper A

10 Tb/s self-homodyne PM-64QAM superchannel transmission with 4% spectral overhead *Journal of Lightwave Technology* ,
DOI: 10.1109/JLT.2018.2820166, 2018

This paper demonstrates self-homodyne detection of a comb-based superchannel using frequency comb regeneration. The regeneration is enabled by transmitting two unmodulated tones which are used in the receiver to regenerate the transmitter comb. The regeneration is implemented using a novel electrical phase-locked loop which enables narrow-band filtering and avoids additional penalty from linewidth scaling. The concept is demonstrated using a 50×20 Gbaud PM-64QAM superchannel with a total throughput of 10 Tb/s. The comb-based regeneration enabled record-low spectral overhead of 4% for self-homodyne detection.

My contribution: I developed the idea of electrical regeneration and, together with A. L-R., built the measurement setup. I wrote the DSP and processed the measurement data. I wrote the paper.

Paper B

High Spectral Efficiency PM-128QAM Comb-Based Superchannel Transmission Enabled by a Single Shared Optical Pilot Tone *Journal of Lightwave Technology* , Vol. 36, no. 6, pp. 1318 - 1325, 2018

This paper demonstrates the use of a single pilot tone to enable the use of blind DSP in superchannels using advanced modulation formats. The single-pilot scheme is shown to facilitate the use of blind DSP while adding minimum spectral overhead. The combination enabled 10.3 bits/s/Hz spectral efficiency for a 54×24 Gbaud PM-128QAM superchannel.

My contribution: I, together with A. L-R. and J. S., developed the idea of the single-pilot scheme and built the measurement setup. I and J. S. wrote the DSP. I did all the measurements and processed the measurement data. I wrote the paper.

Paper C

Comb-Based Superchannel Transmission with Single Shared Optical Pilot Submitted to Optics Express

This paper investigates the proposed single-pilot scheme for transmission distances reaching up to 1000 km. The paper investigates both stability requirements for the transmitter and the receiver comb as well as the sensitivity to distortions on the pilot tone from transmission. The results presented verifies that the single pilot-tone scheme is tolerant to transmission-induced impairments and that DSP complexity reduction can be exploited also for longer distances. The total superchannel spectral efficiency was 9.6 bits/s/Hz (8.4 bits/s/Hz) after 480 (960) km of transmission, respectively.

My contribution: I, together with all co-authors, decided on the the scope of the paper. I built the measurement setup, wrote the DSP and performed all measurements. I wrote the paper.

Paper D

11.5 bits/s/Hz PM-256QAM Comb-Based Superchannel Transmission by Combining Optical and Digital Pilots *Proceedings of the Optical Fiber Conference (OFC)*, Paper. M1G.2, 2018.

This paper exploits the low overhead of the single pilot-tone scheme and combines it with pilot-DSP-based equalization and residual phase-noise tracking to enable detection of PM-256QAM with minimal overhead. Combining three comb-based superchannel covering the full C-band, a record high spectral efficiency of 11.5 bits/s/Hz for is demonstrated, corresponding to 12 bits/s/Hz in achievable information rate.

My contribution: I, with assistance from J. S. built the measurement setup. I wrote the DSP with input from T. Y. I performed all the measurement and analyzed the data. I and J. S. wrote the paper.

References

[1] K. C. Kao and G. A. Hockham, "Dielectric-fibre surface waveguides for optical frequencies", *Proceedings of the Institution of Electrical Engineers*, vol. 113, no. 7, pp. 1151–1158, 1966.

[2] ——, "Dielectric-fibre surface waveguides for optical frequencies", *IEE Proceedings J - Optoelectronics*, vol. 133, no. 3, pp. 191–198, 1986.

[3] R. Mears, L. Reekie, I. Jauncey, and D. Payne, "Low-noise erbium-doped fibre amplifier operating at 1.54μm", *Electronics Letters*, vol. 23, no. 19, p. 1026, 1987.

[4] K. Suzuki, Y. Kimura, and M. Nakazawa, "Pumping wavelength dependence on gain factor of a 0.98 μm pumped Er3+ fiber amplifier", *Applied Physics Letters*, vol. 55, no. 25, pp. 2573–2575, 1989.

[5] R. Laming and D. Payne, "Noise characteristics of erbium-doped fiber amplifier pumped at 980 nm", *IEEE Photonics Technology Letters*, vol. 2, no. 6, pp. 418–421, 1990.

[6] A. Larsson, J. Cody, and R. J. Lang, "Strained-layer InGaAs/GaAs/AlGaAs single quantum well lasers with high internal quantum efficiency", *Applied Physics Letters*, vol. 55, no. 22, pp. 2268–2270, 1989.

[7] A. Larsson, S. Forouhar, J. Cody, R. Lang, and P. Andrekson, "A 980 nm pseudomorphic single quantum well laser for pumping erbium-doped optical fiber amplifiers", *IEEE Photonics Technology Letters*, vol. 2, no. 8, pp. 540–542, 1990.

[8] N. Olsson, P. Andrekson, J. Simpson, T. Tanbun-Ek, R. Logan, and K. Wecht, "Bit-error-rate investigation of two-channel soliton propagation over more than 10 000 km", *Electronics Letters*, vol. 27, no. 9, p. 695, 1991.

[9] P. Andrekson and N. Olsson, "High bit-rate optical soliton communication", in *Global Telecommunications Conference*, 1992, pp. 1880–1885.

[10] L. Cohen, C. Lin, and W. French, "Tailoring zero chromatic dispersion into the 1.5–1.6 μm low-loss spectral region of single-mode fibres", *Electronics Letters*, vol. 15, no. 12, p. 334, 1979.

[11] M. A. Saifi, L. G. Cohen, J. Stone, and S. J. Jang, "Triangular-profile single-mode fiber", *Optics Letters*, vol. 7, no. 1, p. 43, 1982.

[12] B. Ainslie, K. Beales, D. Cooper, C. Day, and J. Rush, "Monomode fibre with ultra-low loss and minimum dispersion at 1.55 μm", *Electronics Letters*, vol. 18, no. 19, p. 842, 1982.

[13] C. D. Poole, K. T. Nelson, J. M. Wiesenfeld, and A. R. McCormick, "Broadband dispersion compensation by using the higher-order spatial mode in a two-mode fiber", *Optics Letters*, vol. 17, no. 14, p. 985, 1992.

[14] J. M. Dugan, A. J. Price, M. Ramadan, D. L. Wolf, E. F. Murphy, A. J. Antos, D. K. Smith, and D. W. Hall, "All-optical, fiber-based 1550 nm dispersion compensation in a 10 Gbit/s, 150 km transmission experiment over 1310 nm optimized fiber", in *Proceedings of Optical Fiber Communication Conference*, paper. PD.14, 1992.

[15] D. Fishman, J. Nagel, T. Cline, R. Tench, T. Pleiss, T. Miller, D. Coult, M. Milbrodt, P. Yeates, A. Chraplyvy, R. Tkach, A. Piccirilli, J. Simpson, and C. Miller, "A high capacity noncoherent FSK lightwave field experiment using Er3+-doped fiber optical amplifiers", *IEEE Photonics Technology Letters*, vol. 2, no. 9, pp. 662–664, 1990.

[16] H. Taga, Y. Yoshida, N. Edagawa, S. Yamamoto, and H. Wakabayashi, "459 km, 2.4 Gbit/s four wavelength multiplexing optical fibre transmission experiment using six Er-doped fibre amplifiers", *Electronics Letters*, vol. 26, no. 8, p. 500, 1990.

[17] D. Marcuse, A. Chraplyvy, and R. Tkach, "Effect of fiber nonlinearity on long-distance transmission", *Journal of Lightwave Technology*, vol. 9, no. 1, pp. 121–128, 1991.

[18] K. S. Kim, W. A. Reed, K. W. Quoi, and R. H. Stolen, "Measurement of the nonlinear index of silica-core and dispersion-shifted fibers", *Optics Letters*, vol. 19, no. 4, p. 257, 1994.

[19] P. Winzer and R.-J. Essiambre, "Advanced optical modulation formats", *Proceedings of the IEEE*, vol. 94, no. 5, pp. 952–985, 2006.

[20] J. McNicol, M. O'Sullivan, K. Roberts, A. Comeau, D. McGhan, and L. Strawczynski, "Electrical domain compensation of optical dispersion optical fibre communication applications", in *Proceedings of Optical Fiber Communication Conference*, paper. OThJ3, 2005.

[21] H. Sun, K.-T. Wu, and K. Roberts, "Real-time measurements of a 40 Gb/s coherent system", *Optics Express*, vol. 16, no. 2, p. 873, 2008.

[22] C. Laperle and M. Osullivan, "Advances in high-speed DACs, ADCs, and DSP for optical coherent transceivers", *Journal of Lightwave Technology*, vol. 32, no. 4, pp. 629–643, 2014.

[23] A. Napoli, M. Mezghanni, T. Rahman, D. Rafique, R. Palmer, B. Spinnler, S. Calabro, C. Carlos, M. Kuschnerov, and M. Bohn, "Digital compensation of bandwidth limitations for high-speed DACs and ADCs", *Journal of Lightwave Technology*, vol. 6, no. 1, p. 1, 2016.

[24] R. Griffin and A. Carter, "Optical differential quadrature phase-shift key (oDQPSK) for high capacity optical transmission", in *Proceedings of Optical Fiber Communication Conference*, paper. WX6, 2002.

[25] C. E. Shannon, "A mathematical theory of communication", *Bell System Technical Journal*, vol. 27, no. 3, pp. 379–423, 1948.

[26] A. Leven and L. Schmalen, "Status and recent advances on forward error correction technologies for lightwave systems", *Journal of Lightwave Technology*, vol. 32, no. 16, pp. 2735–2750, 2014.

[27] K. Kikuchi, "Fundamentals of coherent optical fiber communications", *Journal of Lightwave Technology*, vol. 34, no. 1, pp. 157–179, 2016.

[28] Y. Tamura, H. Sakuma, K. Morita, M. Suzuki, Y. Yamamoto, K. Shimada, Y. Honma, K. Sohma, T. Fujii, and T. Hasegawa, "The first 0.14-dB/km loss optical fiber and its impact on submarine transmission", *Journal of Lightwave Technology*, vol. 36, no. 1, pp. 44–49, 2018.

[29] S. L. Olsson, J. Cho, S. Chandrasekhar, X. Chen, P. J. Winzer, and S. Makovejs, "Probabilistically shaped PDM 4096-QAM transmission over up to 200 km of fiber using standard intradyne detection", *Optics Express*, vol. 26, no. 4, p. 4522, 2018.

[30] M. Terayama, S. Okamoto, K. Kasai, M. Yoshida, and M. Nakazawa, "4096 QAM (72 gbit/s) single-carrier coherent optical transmission with a potential SE of 15.8 bit/s/Hz in all-raman amplified 160 km fiber link", in *Optical Fiber Communication Conference*, paper. Th1F.2, 2018.

[31] S. L. Olsson, J. Cho, S. Chandrasekhar, X. Chen, E. C. Burrows, and P. J. Winzer, "Record-high 17.3-bit/s/Hz spectral efficiency transmission over 50 km using probabilistically shaped PDM 4096-QAM", in *Proceedings of Optical Fiber Communication Conference*, paper. Th4C.5, 2018.

[32] S. Chandrasekhar, B. Li, J. Cho, X. Chen, E. Burrows, G. Raybon, and P. Winzer, "High-spectral-efficiency transmission of PDM 256-QAM with parallel probabilistic shaping at record rate-reach trade-offs", in *Proceedings of European Conference on Optical Communication*, paper. Th.3.C.1, 2016.

[33] L. Beygi, E. Agrell, J. M. Kahn, and M. Karlsson, "Rate-adaptive coded modulation for fiber-optic communications", *Journal of Lightwave Technology*, vol. 32, no. 2, pp. 333–343, 2014.

[34] A. Ghazisaeidi, L. Schmalen, I. F. de Jauregui Ruiz, P. Tran, C. Simonneau, P. Brindel, and G. Charlet, "Transoceanic transmission systems using adaptive multirate FECs", *Journal of Lightwave Technology*, vol. 33, no. 7, pp. 1479–1487, 2015.

[35] T. Fehenberger, A. Alvarado, G. Böcherer, and N. Hanik, "On probabilistic shaping of quadrature amplitude modulation for the nonlinear fiber channel", *Journal of Lightwave Technology*, vol. 34, no. 21, pp. 5063–5073, 2016.

[36] A. Ghazisaeidi, I. F. de Jauregui Ruiz, L. Schmalen, P. Tran, C. Simonneau, E. Awwad, B. Uscumlic, P. Brindel, and G. Charlet, "Submarine transmission systems using digital nonlinear compensation and adaptive rate forward error correction", *Journal of Lightwave Technology*, vol. 34, no. 8, pp. 1886–1895, 2016.

[37] I. F. de Jauregui Ruiz, A. Ghazisaeidi, O. A. Sab, P. Plantady, A. Calsat, S. Dubost, L. Schmalen, V. Letellier, and J. Renaudier, "25.4-Tb/s transmission over transpacific distances using truncated probabilistically shaped PDM-64QAM", *Journal of Lightwave Technology*, vol. 36, no. 6, pp. 1354–1361, 2018.

[38] J.-X. Cai, H. G. Batshon, M. V. Mazurczyk, O. V. Sinkin, D. Wang, M. Paskov, W. W. Patterson, C. R. Davidson, P. C. Corbett, G. M. Wolter, T. E. Hammon, M. A. Bolshtyansky, D. G. Foursa, and A. N. Pilipetskii, "70.46 Tb/s over 7,600 km and 71.65 Tb/s over 6,970 km transmission in C+L band using coded modulation with hybrid constellation shaping and nonlinearity compensation", *Journal of Lightwave Technology*, vol. 36, no. 1, pp. 114–121, 2018.

[39] J.-X. Cai, H. G. Batshon, M. V. Mazurczyk, O. V. Sinkin, D. Wang, M. Paskov, C. R. Davidson, W. W. Patterson, A. Turukhin, M. A. Bolshtyansky, and D. G. Foursa, "51.5 Tb/s capacity over 17,107 km in C+L bandwidth using single-mode fibers and nonlinearity compensation", *Journal of Lightwave Technology*, vol. 36, no. 11, pp. 2135–2141, 2018.

[40] X. Chen, S. Chandrasekhar, S. Randel, G. Raybon, A. Adamiecki, P. Pupalaikis, and P. J. Winzer, "All-electronic 100-GHz bandwidth digital-to-analog converter generating PAM signals up to 190 GBaud", *Journal of Lightwave Technology*, vol. 35, no. 3, pp. 411–417, 2017.

[41] G. Raybon, A. Adamiecki, J. Cho, F. Jorge, A. Konczykowska, M. Riet, B. Duval, J.-Y. Dupuy, N. Fontaine, P. J. Winzer, S. Chandrasekhar, and X. Chen, "180-GBaud all-ETDM single-carrier polarization multiplexed QPSK transmission over 4480 km", in *Proceedings of Optical Fiber Communication Conference*, paper. Th4C.3, 2018.

[42] R. Maher, K. Croussore, M. Lauermann, R. Going, X. Xu, and J. Rahn, "Constellation shaped 66 GBd DP-1024QAM transceiver with 400 km transmission over standard SMF", in *Proceedings of European Conference on Optical Communication*, paper. Th.PDP.B.2, 2017.

[43] R. Going, M. Lauermann, R. Maher, H.-S. Tsai, M. Lu, N. Kim, S. Corzine, P. Studenkov, J. Summers, A. Hosseini, J. Zhang, B. Behnia, J. Tang, S. Buggaveeti, T. Vallaitis, J. Osenbach, M. Kuntz, X. Xu, K. Croussore, V. Lal, P. Evans, J. Rahn, T. Butrie, A. Karanicolas, K.-T. Wu, M. Mitchell, M. Ziari, D. Welch, and F. Kish, "Multi-channel InP-based coherent PICs with hybrid integrated SiGe electronics operating up to 100GBd, 32QAM", in *Proceedings of European Conference on Optical Communication*, 2017.

[44] R.-J. Essiambre, G. Kramer, P. J. Winzer, G. J. Foschini, and B. Goebel, "Capacity limits of optical fiber networks", *Journal of Lightwave Technology*, vol. 28, no. 4, pp. 662–701, 2010.

[45] G. Bosco, P. Poggiolini, A. Carena, V. Curri, and F. Forghieri, "Analytical results on channel capacity in uncompensated optical links with coherent detection", *Optics Express*, vol. 19, no. 26, B440, 2011.

[46] E. Agrell, A. Alvarado, G. Durisi, and M. Karlsson, "Capacity of a nonlinear optical channel with finite memory", *Journal of Lightwave Technology*, vol. 32, no. 16, pp. 2862–2876, 2014.

[47] R. Dar, M. Shtaif, and M. Feder, "New bounds on the capacity of the nonlinear fiber-optic channel", *Optics Letters*, vol. 39, no. 2, p. 398, 2014.

[48] D. J. Richardson, J. M. Fini, and L. E. Nelson, "Space-division multiplexing in optical fibres", *Nature Photonics*, vol. 7, no. 5, pp. 354–362, 2013.

[49] P. J. Winzer and D. T. Neilson, "From scaling disparities to integrated parallelism: A decathlon for a decade", *Journal of Lightwave Technology*, vol. 35, no. 5, pp. 1099–1115, 2017.

[50] D. Soma, Y. Wakayama, S. Beppu, S. Sumita, T. Tsuritani, T. Hayashi, T. Nagashima, M. Suzuki, M. Yoshida, K. Kasai, M. Nakazawa, H. Takahashi, K. Igarashi, I. Morita, and M. Suzuki, "10.16-Peta-bit/s dense SDM/WDM transmission over 6-mode 19-core fiber across the C+L band", *Journal of Lightwave Technology*, vol. 36, no. 6, pp. 1362–1368, 2018.

[51] G. Rademacher, R. S. Luís, B. J. Puttnam, T. A. Eriksson, E. Agrell, R. Maruyama, K. Aikawa, H. Furukawa, Y. Awaji, and N. Wada, "159 Tbit/s C+L band transmission over 1045 km 3-mode graded-index few-mode fiber", in *Proceedings of Optical Fiber Communication Conference*, paper. Th4C.4, 2018.

[52] N. K. Fontaine, R. Ryf, H. Chen, A. V. Benitez, B. Guan, R. Scott, B. Ercan, S. J. B. Yoo, L. E. Grüner-Nielsen, Y. Sun, R. Lingle, E. Antonio-Lopez, and R. Amezcua-Correa, "30x30 MIMO transmission over 15 spatial modes", in *Proceedings of Optical Fiber Communication Conference*, paper. Th5C.1, 2015.

[53] J. van Weerdenburg, R. Ryf, R. Alvarez-Aguirre, N. K. Fontaine, R.-J. Essiambre, H. Chen, J. C. Alvarado-Zacarias, R. Amezcua-Correa, S. Gross, N. Riesen, M. Withford, D. W. Peckham, A. McCurdy, R. Lingle, T. Koonen, and C. Okonkwo, "Mode-multiplexed 16-QAM transmission over 2400-km large-effective-area depressed-cladding 3-mode fiber", in *Proceedings of Optical Fiber Communication Conference*, paper. W4C.2, 2018.

[54] R. Ryf, "Long-haul transmission over multi core fiber with coupled cores", in *Proceedings of European Conference on Optical Communication*, paper. M.2.E.2, 2017.

[55] E. Agrell and M. Karlsson, "Power-efficient modulation formats in coherent transmission systems", *Journal of Lightwave Technology*, vol. 27, no. 22, pp. 5115–5126, 2009.

[56] A. Alvarado and E. Agrell, "Four-dimensional coded modulation with bit-wise decoders for future optical communications", *Journal of Lightwave Technology*, vol. 33, no. 10, pp. 1993–2003, 2015.

[57] D. S. Millar, T. Koike-Akino, K. Kojima, and K. Parsons, "A 24-dimensional modulation format achieving 6 dB asymptotic power efficiency", in *Advanced Photonics*, 2013.

[58] R. Dar, M. Feder, A. Mecozzi, and M. Shtaif, "On shaping gain in the nonlinear fiber-optic channel", in *2014 IEEE International Symposium on Information Theory*, 2014.

[59] X. Liu, S. Chandrasekhar, and P. J. Winzer, "Digital signal processing techniques enabling multi-Tb/s superchannel transmission: An overview of recent advances in DSP-enabled superchannels", *IEEE Signal Processing Magazine*, vol. 31, no. 2, pp. 16–24, 2014.

[60] M. S. Faruk and S. J. Savory, "Digital signal processing for coherent transceivers employing multilevel formats", *Journal of Lightwave Technology*, vol. 35, no. 5, pp. 1125–1141, 2017.

[61] A. Lapidoth, *A Foundation in Digital Communication*. Cambridge University Press, 2009.

[62] R. Walden, "Analog-to-digital converter survey and analysis", *IEEE Journal on Selected Areas in Communications*, vol. 17, no. 4, pp. 539–550, 1999.

[63] A. Pilipetskii, "High-capacity undersea long-haul systems", *IEEE Journal of Selected Topics in Quantum Electronics*, vol. 12, no. 4, pp. 484–496, 2006.

[64] P. Westbergh, R. Safaisini, E. Haglund, A. Larsson, J. Gustavsson, and E. Haglund, "High-speed 850 nm VCSELs operating error free up to 57 gbit/s", *Electronics Letters*, vol. 49, no. 16, pp. 1021–1023, 2013.

[65] M. Zhang, C. Wang, X. Chen, M. Bertrand, A. Shams-Ansari, S. Chandrasekhar, P. Winzer, and M. Lončar, "Ultra-high bandwidth integrated lithium niobate modulators with record-low v_π", in *Proceedings of Optical Fiber Communication Conference*, paper Th4A.5, 2018.

[66] K. Goi, A. Oka, H. Kusaka, Y. Terada, K. Ogawa, T.-Y. Liow, X. Tu, G.-Q. Lo, and D.-L. Kwong, "Low-loss high-speed silicon IQ modulator for QPSK/DQPSK in c and l bands", *Optics Express*, vol. 22, no. 9, p. 10 703, 2014.

[67] Y. Ogiso, H. Wakita, M. Nagatani, H. Yamazaki, M. Nakamura, T. Kobayashi, J. Ozaki, Y. Ueda, S. Nakano, S. Kanazawa, T. Fujii, Y. Hashizume, H. Tanobe, N. Nunoya, M. Ida, Y. Miyamoto, and N. Kikuchi, "Ultra-high bandwidth InP IQ modulator co-assembled with driver IC for beyond 100-GBd CDM", in *Proceedings of Optical Fiber Communication Conference*, 2018.

[68] C. Haffner, W. Heni, Y. Fedoryshyn, J. Niegemann, A. Melikyan, D. L. Elder, B. Baeuerle, Y. Salamin, A. Josten, U. Koch, C. Hoessbacher, F. Ducry, L. Juchli, A. Emboras, D. Hillerkuss, M. Kohl, L. R. Dalton, C. Hafner, and J. Leuthold, "All-plasmonic mach-zehnder modulator enabling optical high-speed communication at the microscale", *Nature Photonics*, vol. 9, no. 8, pp. 525–528, 2015.

[69] C. Haffner, D. Chelladurai, Y. Fedoryshyn, A. Josten, B. Baeuerle, W. Heni, T. Watanabe, T. Cui, B. Cheng, S. Saha, D. L. Elder, L. R. Dalton, A. Boltasseva, V. M. Shalaev, N. Kinsey, and J. Leuthold, "Low-loss plasmon-assisted electro-optic modulator", *Nature*, vol. 556, no. 7702, pp. 483–486, 2018.

[70] Z. Tong, C. Lundström, P. A. Andrekson, C. J. McKinstrie, M. Karlsson, D. J. Blessing, E. Tipsuwannakul, B. J. Puttnam, H. Toda, and L. Gruener-Nielsen, "Towards ultrasensitive optical links enabled by low-noise phase-sensitive amplifiers", *Nature Photonics*, vol. 5, no. 7, pp. 430–436, 2011.

[71] C. Schubert, R. Ludwig, and H.-G. Weber, "High-speed optical signal processing using semiconductor optical amplifiers", *Journal of Optical and Fiber Communications Reports*, vol. 2, no. 2, pp. 171–208, 2005.

[72] G. Agrawal, *Nonlinear Fiber Optics, Fifth Edition (Optics and Photonics)*. Academic Press, 2012.

[73] M. Karlsson, "Transmission systems with low noise phase-sensitive parametric amplifiers", *Journal of Lightwave Technology*, vol. 34, no. 5, pp. 1411–1423, 2016.

[74] P. Poggiolini, A. Carena, V. Curri, G. Bosco, and F. Forghieri, "Analytical modeling of nonlinear propagation in uncompensated optical transmission links", *IEEE Photonics Technology Letters*, vol. 23, no. 11, pp. 742–744, 2011.

[75] P. Poggiolini, G. Bosco, A. Carena, V. Curri, and F. Forghieri, "A simple and accurate model for non-linear propagation effects in uncompensated coherent transmission links", *Proceedings of International Conference on Transparent Optical Networks*, pp. 1–6, 2011.

[76] P. Poggiolini, G. Bosco, A. Carena, V. Curri, Y. Jiang, and F. Forghieri, "The GN-model of fiber non-linear propagation and its applications", *Journal of Lightwave Technology*, vol. 32, no. 4, pp. 694–721, 2014.

[77] A. Nespola, S. Straullu, A. Carena, G. Bosco, R. Cigliutti, V. Curri, P. Poggiolini, M. Hirano, Y. Yamamoto, T. Sasaki, J. Bauwelinck, K. Verheyen, and F. Forghieri, "GN-model validation over seven fiber types in uncompensated PM-16QAM Nyquist-WDM links", *IEEE Photonics Technology Letters*, vol. 26, no. 2, pp. 206–209, 2014.

[78] A. Carena, G. Bosco, V. Curri, Y. Jiang, P. Poggiolini, and F. Forghieri, "EGN model of non-linear fiber propagation", *Optics Express*, vol. 22, no. 13, pp. 16 335–16 362, 2014.

[79] J. P. Gordon and H. Kogelnik, "PMD fundamentals: Polarization mode dispersion in optical fibers", *Proceedings of the National Academy of Sciences*, vol. 97, no. 9, pp. 4541–4550, 2000.

[80] M. Karlsson and H. Sunnerud, "Effects of nonlinearities on PMD-induced system impairments", *Journal of Lightwave Technology*, vol. 24, no. 11, pp. 4127–4137, 2006.

[81] M. Karlsson, "Geometrical interpretation of second-order PMD", *Journal of Lightwave Technology*, vol. 24, no. 1, pp. 643–651, 2006.

[82] D. H. Goldstein, *Polarized Light, Third Edition*. CRC Press, 2010.

[83] P. K. A. Wai and C. R. Menyuk, "Polarization mode dispersion, decorrelation, and diffusion in optical fibers with randomly varying birefringence", *Journal of Lightwave Technology*, vol. 14, no. 2, pp. 148–157, 1996.

[84] E. Ip, A. P. T. Lau, D. J. F. Barros, and J. M. Kahn, "Coherent detection in optical fiber systems", *Optics Express*, vol. 16, no. 2, p. 753, 2008.

[85] G. Bosco, S. M. Bilal, A. Nespola, P. Poggiolini, and F. Forghieri, "Impact of the transmitter IQ-skew in multi-subcarrier coherent optical systems", in *Proceedings of Optical Fiber Communication Conference*, paper. W4A.5, 2016.

[86] E. P. da Silva and D. Zibar, "Widely linear equalization for IQ imbalance and skew compensation in optical coherent receivers", *Journal of Lightwave Technology*, vol. 34, no. 15, pp. 3577–3586, 2016.

[87] C. R. S. Fludger and T. Kupfer, "Transmitter impairment mitigation and monitoring for high baud-rate, high order modulation systems", in *Proceedings of European Conference on Optical Communication*, paper. Tu.2.A.2, 2016.

[88] W. Cheney and D. R. Kincaid, *Linear Algebra: Theory And Applications*. Jones & Bartlett Learning, 2008.

[89] S. J. Savory, "Digital filters for coherent optical receivers", *Optics Express*, vol. 16, no. 2, p. 804, 2008.

[90] I. Tomkos, S. Azodolmolky, J. Sole-Pareta, D. Careglio, and E. Palkopoulou, "A tutorial on the flexible optical networking paradigm: State of the art, trends, and research challenges", *Proceedings of the IEEE*, vol. 102, no. 9, pp. 1317–1337, 2014.

[91] H. Wymeersch and P. Johannisson, "Maximum-likelihood-based blind dispersion estimation for coherent optical communication", *Journal of Lightwave Technology*, vol. 30, no. 18, pp. 2976–2982, 2012.

[92] S. Yao, T. A. Eriksson, S. Fu, P. Johannisson, M. Karlsson, P. A. Andrekson, T. Ming, and D. Liu, "Fast and robust chromatic dispersion estimation based on temporal auto-correlation after digital spectrum superposition", *Optics Express*, vol. 23, no. 12, p. 15 418, 2015.

[93] J. C. Diniz, E. P. da Silva, M. Piels, and D. Zibar, "Joint IQ skew and chromatic dispersion estimation for coherent optical communication receivers", in *Advanced Photonics*, 2016.

[94] R. W. Schafer and A. V. Oppenheim, *Discrete-Time Signal Processing: Pearson New International Edition*. Pearson Education Limited, 2013.

[95] R. Kudo, T. Kobayashi, K. Ishihara, Y. Takatori, a. Sano, and Y. Miyamoto, "Coherent optical single carrier transmission using overlap frequency domain equalization for long-haul optical systems", *Journal of Lightwave Technology*, vol. 27, no. 16, pp. 3721–3728, 2009.

[96] R. Ryf, S. Randel, A. H. Gnauck, C. Bolle, A. Sierra, S. Mumtaz, M. Esmaeelpour, E. C. Burrows, R.-J. Essiambre, P. J. Winzer, D. W. Peckham, A. H. McCurdy, and R. Lingle, "Mode-division multiplexing over 96 km of few-mode fiber using coherent 6x6 MIMO processing", *Journal of Lightwave Technology*, vol. 30, no. 4, pp. 521–531, 2012.

[97] S. Ö. Arik, D. Askarov, and J. M. Kahn, "Effect of mode coupling on signal processing complexity in mode-division multiplexing", *Journal of Lightwave Technology*, vol. 31, no. 3, pp. 423–431, 2013.

[98] S. O. Haykin, *Adaptive Filter Theory (5th Edition)*. Pearson, 2013.

[99] M. Kuschnerov, M. Chouayakh, K. Piyawanno, B. Spinnler, E. de Man, P. Kainzmaier, M. S. Alfiad, A. Napoli, and B. Lankl, "Data-aided versus blind single-carrier coherent receivers", *IEEE Photonics Journal*, vol. 2, no. 3, pp. 387–403, 2010.

[100] R. Johnson, P. Schniter, T. Endres, J. Behm, D. Brown, and R. Casas, "Blind equalization using the constant modulus criterion: A review", *Proceedings of the IEEE*, vol. 86, no. 10, pp. 1927–1950, 1998.

[101] A.-J. van der Veen and A. Paulraj, "An analytical constant modulus algorithm", *IEEE Transactions on Signal Processing*, vol. 44, no. 5, pp. 1136–1155, 1996.

[102] I. Fatadin, D. Ives, and S. Savory, "Blind Equalization and Carrier Phase Recovery in a 16-QAM Optical Coherent System", *Journal of Lightwave Technology*, vol. 27, no. 15, pp. 3042–3049, 2009.

[103] M. Ready and R. Gooch, "Blind equalization based on radius directed adaptation", in *International Conference on Acoustics, Speech, and Signal Processing*, 1990.

[104] D. Ashmawy, K. Banovic, E. Abdel-Raheem, M. Youssif, H. Mansour, and M. Mohanna, "Joint MCMA and DD blind equalization algorithm with variable-step size", in *IEEE International Conference on Electro/Information Technology*, 2009.

[105] J. M. Filho, M. T. M. Silva, and M. D. Miranda, "A family of algorithms for blind equalization of QAM signals", in *IEEE International Conference on Acoustics, Speech and Signal Processing*, 2011.

[106] E. Ip and J. M. Kahn, "Feedforward carrier recovery for coherent optical communications", *Journal of Lightwave Technology*, vol. 25, no. 9, pp. 2675–2692, 2007.

[107] J. C. M. Diniz, J. C. R. F. de Oliveira, E. S. Rosa, V. B. Ribeiro, V. E. S. Parahyba, R. da Silva, E. P. da Silva, L. H. H. de Carvalho, A. F. Herbster, and A. C. Bordonalli, "Simple feed-forward wide-range frequency offset estimator for optical coherent receivers", *Optics Express*, vol. 19, no. 26, B323, 2011.

[108] Y. Liu, Y. Peng, S. Wang, and Z. Chen, "Improved FFT-based frequency offset estimation algorithm for coherent optical systems", *IEEE Photonics Technology Letters*, vol. 26, no. 6, pp. 613–616, 2014.

[109] F. Xiao, J. Lu, S. Fu, C. Xie, M. Tang, J. Tian, and D. Liu, "Feed-forward frequency offset estimation for 32-QAM optical coherent detection", *Optics Express*, vol. 25, no. 8, p. 8828, 2017.

[110] J. Lu, X. Li, S. Fu, M. Luo, M. Xiang, H. Zhou, M. Tang, and D. Liu, "Joint carrier phase and frequency-offset estimation with parallel implementation for dual-polarization coherent receiver", *Optics Express*, vol. 25, no. 5, p. 5217, 2017.

[111] A. Meiyappan, P. Y. Kam, and H. Kim, "On decision aided carrier phase and frequency offset estimation in coherent optical receivers", *Journal of Lightwave Technology*, vol. 31, no. 13, pp. 2055–2069, 2013.

[112] M. Selmi, Y. Jaouen, and P. Ciblat, "Accurate digital frequency offset estimator for coherent PolMux QAM transmission systems", in *Proceedings of European Conference on Optical Communication*, paper. P3.08, 2009.

[113] G. Liu, K. Zhang, R. Zhang, R. Proietti, H. Lu, and S. J. B. Yoo, "Demonstration of a carrier frequency offset estimator for 16-/32-QAM coherent receivers: A hardware perspective", *Optics Express*, vol. 26, no. 4, p. 4853, 2018.

[114] I. Fatadin, D. Ives, and S. J. Savory, "Carrier phase recovery for 16-QAM using QPSK partitioning and sliding window averaging", *IEEE Photonics Technology Letters*, vol. 26, no. 9, pp. 854–857, 2014.

[115] A. Viterbi, "Nonlinear estimation of PSK-modulated carrier phase with application to burst digital transmission", *IEEE Transactions on Information Theory*, vol. 29, no. 4, pp. 543–551, 1983.

[116] Y. Gao, A. P. T. Lau, S. Yan, and C. Lu, "Low-complexity and phase noise tolerant carrier phase estimation for dual-polarization 16-QAM systems", *Optics Express*, vol. 19, no. 22, pp. 21 717–21 729, 2011.

[117] M. G. Taylor, "Phase estimation methods for optical coherent detection using digital signal processing", *Journal of Lightwave Technology*, vol. 27, no. 7, pp. 901–914, 2009.

[118] I. Fatadin, D. Ives, and S. J. Savory, "Laser linewidth tolerance for 16-QAM coherent optical systems using QPSK partitioning", *IEEE Photonics Technology Letters*, vol. 22, no. 9, pp. 631–633, 2010.

[119] T. Pfau, S. Hoffmann, and R. Noé, "Hardware-efficient coherent digital receiver concept with feedforward carrier recovery for M-QAM constellations", *Journal of Lightwave Technology*, vol. 27, no. 8, pp. 989–999, 2009.

[120] X. Zhou, "An improved feed-forward carrier recovery algorithm for coherent receivers with M-QAM modulation format", *IEEE Photonics Technology Letters*, vol. 22, no. 14, pp. 1051–1053, 2010.

[121] T. Adali, P. J. Schreier, and L. L. Scharf, "Complex-valued signal processing: The proper way to deal with impropriety", *IEEE Transactions on Signal Processing*, vol. 59, no. 11, pp. 5101–5125, 2011.

[122] D. S. Millar, R. Maher, D. Lavery, T. Koike-Akino, M. Pajovic, A. Alvarado, M. Paskov, K. Kojima, K. Parsons, B. C. Thomsen, S. J. Savory, and P. Bayvel, "Design of a 1 Tb/s superchannel coherent receiver", *Journal of Lightwave Technology*, vol. 34, no. 6, pp. 1453–1463, 2016.

[123] R. Elschner, F. Frey, C. Meuer, J. K. Fischer, S. Alreesh, C. Schmidt-Langhorst, L. Molle, T. Tanimura, and C. Schubert, "Experimental demonstration of a format-flexible single-carrier coherent receiver using data-aided digital signal processing.", *Optics Express*, vol. 20, no. 27, p. 6, 2012.

[124] G. Bosco, "Flexible transceivers and the rate/reach trade-off", in *Proceedings of Optical Fiber Communication Conference*, paper. M1G.1, 2018.

[125] A. Alvarado, E. Agrell, D. Lavery, R. Maher, and P. Bayvel, "Replacing the soft-decision FEC limit paradigm in the design of optical communication systems", *Journal of Lightwave Technology*, vol. 34, no. 2, pp. 707–721, 2016.

[126] A. Alvarado, T. Fehenberger, B. Chen, and F. M. J. Willems, "Achievable information rates for fiber optics: Applications and computations", *Journal of Lightwave Technology*, pp. 1–1, 2018.

[127] V. Torres-Company and A. M. Weiner, "Optical frequency comb technology for ultra-broadband radio-frequency photonics", *Laser & Photonics Reviews*, vol. 8, no. 3, pp. 368–393, 2013.

[128] H. Haus, "Mode-locking of lasers", *IEEE Journal of Selected Topics in Quantum Electronics*, vol. 6, no. 6, pp. 1173–1185, 2000.

[129] P. Marin-Palomo, J. N. Kemal, M. Karpov, A. Kordts, J. Pfeifle, M. H. Pfeiffer, P. Trocha, S. Wolf, V. Brasch, M. H. Anderson, R. Rosenberger, V. Kovendhan, W. Freude, T. J. Kippenberg, and C. Koos, "Microresonator-based solitons for massively parallel coherent optical communications", *Nature*, vol. 546, no. 7657, pp. 274–279, 2017.

[130] V. Ataie, E. Myslivets, B. P.-P. Kuo, N. Alic, and S. Radic, "Spectrally equalized frequency comb generation in multistage parametric mixer with nonlinear pulse shaping", *Journal of Lightwave Technology*, vol. 32, no. 4, pp. 840–846, 2014.

[131] V. Durán, S. Tainta, and V. Torres-Company, "Ultrafast electrooptic dual-comb interferometry", *Optics Express*, vol. 23, no. 23, p. 30 557, 2015.

[132] G. Ycas, F. R. Giorgetta, E. Baumann, I. Coddington, D. Herman, S. A. Diddams, and N. R. Newbury, "High-coherence mid-infrared dual-comb spectroscopy spanning 2.6 to 5.2 μm", *Nature Photonics*, vol. 12, no. 4, pp. 202–208, 2018.

[133] S. T. Cundiff and A. M. Weiner, "Optical arbitrary waveform generation", *Nature Photonics*, vol. 4, no. 11, pp. 760–766, 2010.

[134] D. T. Spencer, T. Drake, T. C. Briles, J. Stone, L. C. Sinclair, C. Fredrick, Q. Li, D. Westly, B. R. Ilic, A. Bluestone, N. Volet, T. Komljenovic, L. Chang, S. H. Lee, D. Y. Oh, M.-G. Suh, K. Y. Yang, M. H. P. Pfeiffer, T. J. Kippenberg, E. Norberg, L. Theogarajan, K. Vahala, N. R. Newbury, K. Srinivasan, J. E. Bowers, S. A. Diddams, and S. B. Papp, "An optical-frequency synthesizer using integrated photonics", *Nature*, 2018.

[135] A. J. Metcalf, V. Torres-Company, D. E. Leaird, and A. M. Weiner, "High-power broadly tunable electrooptic frequency comb generator", *Journal of Selected Topics in Quantum Electronics*, vol. 19, no. 6, pp. 231–236, 2013.

[136] V. Torres-Company, J. Lancis, and P. Andrés, "Lossless equalization of frequency combs", *Optics Letters*, vol. 33, no. 16, p. 1822, 2008.

[137] J. N. Kemal, J. Pfeifle, P. Marin-Palomo, M. D. G. Pascual, S. Wolf, F. Smyth, W. Freude, and C. Koos, "Multi-wavelength coherent transmission using an optical frequency comb as a local oscillator", *Optics Express*, vol. 24, no. 22, pp. 25 432–25 445, 2016.

[138] M. Fujiwara, J. Kani, H. Suzuki, K. Araya, and M. Teshima, "Flattened optical multicarrier generation of 12.5 GHz spaced 256 channels based on sinusoidal amplitude and phase hybrid modulation", *Electronics Letters*, vol. 37, no. 15, pp. 967–968, 2001.

[139] V. Ataie, E. Temprana, L. Liu, E. Myslivets, B. P.-P. Kuo, N. Alic, and S. Radic, "Ultrahigh count coherent WDM channels transmission using optical parametric comb-based frequency synthesizer", *Journal of Lightwave Technology*, vol. 33, no. 3, pp. 694–699, 2015.

[140] J. Pfeifle, V. Brasch, M. Lauermann, Y. Yu, D. Wegner, T. Herr, K. Hartinger, P. Schindler, J. Li, D. Hillerkuss, R. Schmogrow, C. Weimann, R. Holzwarth, W. Freude, J. Leuthold, T. J. Kippenberg, and C. Koos, "Coherent terabit communications with microresonator Kerr frequency combs", *Nature Photonics*, vol. 8, no. 5, pp. 375–380, 2014.

[141] A. Fülöp, M. Mazur, A. Lorences-Riesgo, T. A. Eriksson, P.-H. Wang, Y. Xuan, D. E. Leaird, M. Qi, P. A. Andrekson, A. M. Weiner, and V. Torres-Company, "Long-haul coherent communications using microresonator-based frequency combs", *Optics Express*, vol. 25, no. 22, p. 26 678, 2017.

[142] A. Fülöp, M. Mazur, A. Lorences-Riesgo, Ó. B. Helgason, P.-H. Wang, Y. Xuan, D. E. Leaird, M. Qi, P. A. Andrekson, A. M. Weiner, and V. Torres-Company, "High-order coherent communications using mode-locked dark-pulse kerr combs from microresonators", *Nature Communications*, vol. 9, no. 1, 2018.

[143] P. Delfyett, S. Gee, M.-T. Choi, H. Izadpanah, W. Lee, S. Ozharar, F. Quinlan, and T. Yilmaz, "Optical frequency combs from semiconductor lasers and applications in ultrawideband signal processing and communications", *Journal of Lightwave Technology*, vol. 24, no. 7, pp. 2701–2719, 2006.

[144] J. N. Kemal, P. Marin-Palomo, K. Merghem, A. Guy, cosimo calo, R. Brenot, F. Lelarge, A. Ramdane, S. Randel, W. Freude, and C. Koos, "32QAM WDM transmission using a quantum-dash passively mode-locked laser with resonant feedback", in *Proceedings of Optical Fiber Communication Conference*, paper. Th5C.3, 2017.

[145] W. Mao, P. A. Andrekson, and J. Toulouse, "Investigation of a spectrally flat multi-wavelength dwdm source based on optical phase- and intensity-modulation", in *Proceedings of Optical Fiber Communication Conference*, paper. MF78, vol. 1, 2004, pp. 235–.

[146] B. P.-P. Kuo, E. Myslivets, V. Ataie, E. G. Temprana, N. Alic, and S. Radic, "Wideband parametric frequency comb as coherent optical carrier", *Journal of Lightwave Technology*, vol. 31, no. 21, pp. 3414–3419, 2013.

[147] B. Puttnam, R. Luis, W. Klaus, J. Sakaguchi, J.-M. D. Mendinueta, Y. Awaji, N. Wada, Y. Tamura, T. Hayashi, M. Hirano, and M. J., "2.15 Pb/s transmission using a 22 core homogeneous single-mode multi-core fiber and wideband optical comb", in *Proceedings of European Conference on Optical Communication*, paper. PDP3.1, 2015.

[148] E. Temprana, B.-P. Kuo, N. Alic, S. Radic, and S. Grubb, "400 gb/s WDM DP-256-QAM transmission with 50 GHz channel separation", in *IEEE Photonics Conference*, 2016.

[149] E. Temprana, E. Myslivets, B. P.-. P. Kuo, L. Liu, V. Ataie, N. Alic, and S. Radic, "Overcoming kerr-induced capacity limit in optical fiber transmission", *Science*, vol. 348, no. 6242, pp. 1445–1448, 2015.

[150] E. Temprana, E. Myslivets, L. Liu, V. Ataie, A. Wiberg, B. Kuo, N. Alic, and S. Radic, "Two-fold transmission reach enhancement enabled by transmitter-side digital backpropagation and optical frequency comb-derived information carriers", *Optics Express*, vol. 23, no. 16, p. 20 774, 2015.

[151] L. Lundberg, M. Mazur, A. Lorences-Riesgo, M. Karlsson, and P. A. Andrekson, "Joint carrier recovery for DSP complexity reduction in frequency comb-based superchannel transceivers", in *Proceedings of European Conference on Optical Communication*, paper. Th.1.D.3, 2017.

[152] T. Miyazaki and F. Kubota, "PSK self-homodyne detection using a pilot carrier for multibit/symbol transmission with inverse-RZ signal", *IEEE Photonics Technology Letters*, vol. 17, no. 6, pp. 1334–1336, 2005.

[153] M. Sjodin, P. Johannisson, M. Karlsson, Z. Tong, and P. A. Andrekson, "OSNR requirements for self-homodyne coherent systems", *IEEE Photonics Technology Letters*, vol. 22, no. 2, pp. 91–93, 2010.

[154] P. Johannisson, M. Sjodin, M. Karlsson, E. Tipsuwannakul, and P. Andrekson, "Cancellation of nonlinear phase distortion in self-homodyne coherent systems", *IEEE Photonics Technology Letters*, vol. 22, no. 11, pp. 802–804, 2010.

[155] M. Sjödin, E. Agrell, P. Johannisson, G.-W. Lu, P. A. Andrekson, and M. Karlsson, "Filter optimization for self-homodyne coherent WDM systems using interleaved polarization division multiplexing", *Journal of Lightwave Technology*, vol. 29, no. 9, pp. 1219–1226, 2011.

[156] B. J. Puttnam, R. S. Luis, J. M. Delgado Mendinueta, J. Sakaguchi, W. Klaus, Y. Kamio, M. Nakamura, N. Wada, Y. Awaji, A. Kanno, K. Tetsuya, and M. Tetsuya, "Self-homodyne detection in optical communication systems", in *Photonics*, vol. 1, 2014, pp. 110–130.

[157] B. J. Puttnam, J. Sakaguchi, J. M. D. Mendinueta, W. Klaus, Y. Awaji, N. Wada, A. Kanno, and T. Kawanishi, "Investigating self-homodyne coherent detection in a 19 channel space-division-multiplexed transmission link", *Optics Express*, vol. 21, no. 2, pp. 1561–1566, 2013.

[158] B. J. Puttnam, R. Luis, J.-M. Delgado-Mendinueta, J. Sakaguchi, W. Klaus, Y. Awaji, N. Wada, A. Kanno, and T. Kawanishi, "High-capacity self-homodyne PDM-WDM-SDM transmission in a 19-core fiber", *Optics Express*, vol. 22, no. 18, p. 21 185, 2014.

[159] R. S. Luis, B. J. Puttnam, A. V. T. Cartaxo, W. Klaus, J. M. D. Mendinueta, Y. Awaji, N. Wada, T. Nakanishi, T. Hayashi, and T. Sasaki, "Time and modulation frequency dependence of crosstalk in homogeneous multi-core fibers", *Journal of Lightwave Technology*, vol. 34, no. 2, pp. 441–447, 2016.

[160] A. C. Bordonalli, M. J. Fice, and A. J. Seeds, "Optical injection locking to optical frequency combs for superchannel coherent detection", *Optics Express*, vol. 23, no. 2, pp. 1547–1557, 2015.

[161] A. Lorences-Riesgo, T. A. Eriksson, A. Fülöp, P. A. Andrekson, and M. Karlsson, "Frequency-comb regeneration for self-homodyne superchannels", *Journal of Lightwave Technology*, vol. 34, no. 8, pp. 1800–1806, 2016.

[162] A. Lorences-Riesgo, M. Mazur, T. A. Eriksson, P. A. Andrekson, and M. Karlsson, "Self-homodyne 24x32-QAM superchannel receiver enabled by all-optical comb regeneration using Brillouin amplification", *Optics Express*, vol. 24, no. 26, pp. 29 714–29 723, 2016.